Wirelessly Powered Two-Way Communication With Nonlinear Energy Harvesting Model: Rate Regions Under Fixed and Mobile Relay

Shuai Wang, *Student Member, IEEE*, Minghua Xia, *Member, IEEE*, Kaibin Huang, *Senior Member, IEEE*, and Yik-Chung Wu, *Senior Member, IEEE*

***Abstract*— While two-way communication can improve the spectral efficiency of wireless networks, distances from the relay to the two users are usually asymmetric, leading to excessive wireless energy at the nearby user. To exploit the excessive energy, energy harvesting at user terminals is a viable option. Unfortunately, the exact gain brought by wireless power transfer (WPT) in two-way communication is currently unknown. To fill this gap, in this paper, the achievable rate region of wirelessly powered two-way communication with a fixed relay is derived. Not only this newly established result is shown to enclose the existing achievable rate region of two-way relay channel without energy harvesting but also the gain is precisely quantified. On the other hand, it is well-known that a major obstacle to WPT is the path-loss. By endowing the relay with mobility, the distances between the relay and users can be varied, thus providing a potential solution to combat pathloss at the expense of energy for transmission. To characterize the consequence brought by such a scheme, a pair of inner and outer bounds to the achievable rate region of wirelessly powered two-way communication under a mobile relay is further derived. By comparing the exact achievable rate region for the fixed relay case and the achievable rate bounds for the mobile relay case, it is possible to quantify the relative advantage of spending energy on moving versus on transmission in wirelessly powered two-way communication.**

***Index Terms*— Achievable rate region, two-way relay channel (TWRC), wireless power transfer (WPT), beamforming design, unmanned ground vehicle (UGV), mobile relay, nonlinear energy harvesting model, Powercast P2110.**

Manuscript received March 01, 2017; revised June 13, 2017 and August 06, 2017; accepted September 24, 2017. Date of publication October 6, 2017; date of current version December 8, 2017. This work was supported in part by the National Natural Science Foundation of China under Grant 61671488, in part by the Special Fund for Science and Technology Development in Guangdong province under Grant 2016A050503025, in part by the Fundamental Research Funds for the Central Universities of China under Grant 161gzd03, and in part by the HKU Seed Funding Programme under Project 201611159019. The work of K. Huang was supported by Hong Kong Research Grants Council under Grant 17209917 and Grant 17259416. The associate editor coordinating the review of this paper and approving it for publication was A. Bletsas. *(Corresponding author: Shuai Wang.)*

S. Wang, K. Huang, and Y.-C. Wu are with the Department of Electrical and Electronic Engineering, The University of Hong Kong, Hong Kong (e-mail: swang@eee.hku.hk; huangkb@eee.hku.hk; ycwu@eee.hku.hk).

M. Xia is with the School of Electronics and Information Technology, Sun Yat-sen University, Guangzhou 510006, China (e-mail: xiamingh@mail.sysu.edu.cn).

Color versions of one or more of the figures in this paper are available online at http://ieeexplore.ieee.org.

Digital Object Identifier 10.1109/TWC.2017.2758767

I. Introduction

A. Motivation

TWO-WAY communication takes place in a three-node network, where two users exchange information via the relay station. In practice, the distances from the relay to the two users are usually asymmetric [1], leading to excessive wireless energy at the closer user [2]. In order to salvage this excessive energy, wireless power transfer (WPT) can be exploited if user terminals are equipped with energy harvesters [3]–[5]. With the harvested energy, the users are able to increase their subsequent uplink transmit powers and thus improve their communication performance [6]–[12]. Therefore, wirelessly powered two-way communication provides a promising solution for cooperative sensor networks, where low-cost sensors need to exchange data to jointly complete tasks such as localization [13] and anomaly detection [14].

In order to evaluate the performance gain brought by WPT in two-way relay channel (TWRC), a characterization of its achievable rate region is fundamental. The rate region defines not only the set of all achievable rate combinations, but also the performance trade-off between the two user terminals [15]. While existing achievable rate regions of TWRC have been studied under various transmission policies (e.g., decode-and-forward scheme [16], amplify-and-forward scheme [17], [18], and compute-and-forward scheme [19], [20]), they are not applicable to the wirelessly powered TWRC and the achievable rate region of wirelessly powered two-way relay system needs further investigation.

For wirelessly powered TWRC, a major obstacle is the distance-dependent path-loss during energy transmission [3]. To reduce the effect of path-loss, this paper further investigates a viable solution that the relay is mounted on an unmanned ground vehicle (UGV). With such a scheme, the moving relay could vary its location at the expense of transmission energy, but has the flexibility of being close to different energy harvesting users at different times. In contrast to the aerial vehicle that needs high energy consumption just to keep its location unchanged [21], the UGV relay has a low power cost when stopping to serve users [22]–[25]. This makes it attractive for extensive applications such as sensor networks [24], indoor small cells, and Internet of things [26]. However, as the relay is capable of moving, the achievable rate region of UGV-based wirelessly powered TWRC is dependent on the relay moving

trajectory and the stopping time at each point along the trajectory, which leads to a more complicated situation than the fixed relay case. As a result, it is important to derive new theoretical results for the UGV two-way relay system.

B. Challenges and Contributions

Since the wirelessly powered TWRC involves two users' data-rates, finding the achievable rate region is a multi-objective optimization problem. This multi-objective problem involves optimization of uplink-downlink beamformers at relay, which is challenging even for the special case of fixed relay due to the pairwise uplink-downlink coupling [2]. More specifically, in wirelessly powered TWRC, a single transmit beamformer at relay controls both users' downlink information and power transfer. As the downlink power transfer further affects both users' subsequent uplink information transfer, an adjustment of the transmit beamformer at relay would simultaneously impact four transmission links, thus significantly varying the rate region.

For fixed relay, a traditional way to resolve such pairwise uplink-downlink coupling is to apply semidefinite programming [2], and the optimal beamforming design can only be obtained numerically. In contrast, this paper presents a closed-form optimal beamforming solution, and by using a simple bisection search algorithm, the exact achievable rate region of wirelessly powered TWRC with a fixed relay is obtained. It is shown that the newly established achievable rate region encloses the existing rate region without energy harvesting [19], and for the first time, the performance gain in TWRC brought by energy harvesting is concisely quantified.

On the other hand, when the relay is moving along a predefined trajectory, finding the achievable rate region becomes even more challenging. This is because not only the stopping times at different locations along the trajectory need to be determined, but also the beamformers at relay and power splitters at users at each location are jointly optimized. Furthermore, since the harvested energy at users can be stored in batteries, the wireless power transfer at previous locations might have a long-term impact on subsequent locations. Consequently, compared to the fixed relay case, the dimension of design variables is significantly increased and the resultant problem involves an additional nonlinear coupling between time allocation and uplink-downlink beamformers. In order to get around the above challenges, a pair of tight inner and outer bounds of the exact achievable rate region for the wirelessly powered TWRC with mobile relay is derived, using majorization and relaxation, respectively. Finally, it is found that the derived rate bounds are highly dependent on the relay movement trajectory, and the proposed algorithms can concisely quantify the performance gain/loss brought by moving the relay at the expense of transmission energy.

C. Organization

The rest of the paper is organized as follows. In Section II, the system model is described, and the achievable rate region problem is formulated in Section III. In Section IV, the exact achievable rate region is derived for the wirelessly powered TWRC with a fixed relay. In Section V, the inner and outer rate region bounds are obtained for the wirelessly powered TWRC with a moving relay. Finally, numerical results are presented in Section VI, and conclusions are drawn in Section VII.

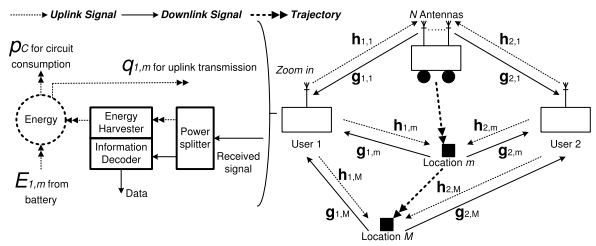

Fig. 1. System model of wirelessly powered TWRC with a UGV relay.

Notation: Italic letters, simple bold letters, and capital bold letters represent scalars, vectors, and matrices, respectively. The operators $\mathrm{Tr}(\cdot)$, $(\cdot)^T$, $(\cdot)^H$, $\mathrm{Rank}(\cdot)$, $(\cdot)^{-1}$ take the trace, transpose, Hermitian, rank, and inverse of a matrix, respectively, while $\mathrm{vec}(\cdot)$ is the matrix vectorization operator. Symbol $\mathbf{I}_N$ represents the $N \times N$ identity matrix. The operators $[x]^+ = \max(x, 0)$ and $[x]^- = \min(x, 0)$. Finally, $\mathbb{E}(\cdot)$ represents the expectation of a random variable and $\exp(\cdot)$ represents the exponential function of a scalar.

II. System Model

A. Relay Movement

We consider a TWRC consisting of a mobile relay with N antennas, and 2 single-antenna users. As shown in Fig. 1, the two users intend to exchange messages with each other through the relay while the relay is moving along a predefined trajectory within a time duration T (for the special case of fixed relay, the length of trajectory is simply zero). In particular, from the starting point $m = 1$, the relay stops for a duration $2t_1$ and then it moves to point $m = 2$, and stops for a duration $2t_2$. The relay keeps on moving and stopping along the trajectory until it reaches the destination $m = M$. Based on such a model, the moving time s_m from the m^{th} to the $(m+1)^{\text{th}}$ point is $s_m = D_m/v$ with D_m being the distance between the two points and v being the velocity. As the relay has to move from point $m = 1$ to point $m = M$ within the duration T, we have $\sum_{m=1}^{M}(2t_m + s_m) = T$, where $s_M = 0$ due to the M^{th} point being the destination. Furthermore, since the total motion energy E_G of the relay is proportional to the total motion time [22]–[24], it can be expressed in the form of

$$E_G = (\lambda_1 + \lambda_2 v) \sum_{m=1}^{M} s_m, \tag{1}$$

where λ_1 and λ_2 are parameters of the model (e.g., for a Pioneer 3DX robot, $\lambda_1 = 0.29$ and $\lambda_2 = 7.4$ [23, Sec. IV-C]).

At each stopping point, lattice code based compute-and-forward network coding is used to accomplish the two-way communications, since the lattice-based two-way relaying achieves a larger achievable rate region than the amplify-and-forward scheme, at the expense of slightly higher complexity [19]. Furthermore, the system is assumed to operate in a half-duplex mode, i.e., the uplink and downlink each takes t_m for transmission.[1] Below, we give the details of the

[1]The derivations in this paper can be readily extended to the full duplex case.

uplink and downlink signal models when the relay is at the m^{th} stopping point.

B. Uplink Signal Model

For the uplink transmission, user i transmits a vector $\mathbf{x}_{i,m} \in \mathbb{C}^{L_m \times 1}$ to the relay, with $i \in \{1, 2\}$, $m \in \{1, \ldots, M\}$, and L_m being the number of symbols. The $\mathbf{x}_{i,m}$ is generated from the pre-determined lattice code (details documented in [2, Appendix A]) and the user transmit power is $q_{i,m} = \frac{1}{t_m}\mathbb{E}[||\mathbf{x}_{i,m}||^2]$. Then, the received signal $\mathbf{Y}_m \in \mathbb{C}^{N \times L_m}$ at the relay is given by $\mathbf{Y}_m = \mathbf{h}_{1,m}\mathbf{x}_{1,m}^T + \mathbf{h}_{2,m}\mathbf{x}_{2,m}^T + \mathbf{N}_m$, where $\mathbf{h}_{i,m} \in \mathbb{C}^{N \times 1}$ denotes the uplink channel vector[2] of user i, and $\mathbf{N}_m \in \mathbb{C}^{N \times L_m}$ is the Gaussian noise with $\mathbb{E}[\text{vec}(\mathbf{N}_m)\text{vec}(\mathbf{N}_m)^H] = \sigma_r^2 \mathbf{I}_{NL_m}$. Applying a receive beamformer $\mathbf{w}_m^H$ (with $||\mathbf{w}_m|| = 1$) to $\mathbf{Y}_m$, the uplink signal-to-noise ratio (SNR) of user i is $q_{i,m}|\mathbf{w}_m^H\mathbf{h}_{i,m}|^2/\sigma_r^2$. Using the uplink SNR and the results from [19, Th. 3], the uplink achievable rate $R_{i,m}^{\text{UL}}$ from user i to the relay can be computed to be

$$R_{i,m}^{\text{UL}} = \left[\log_2\left(\frac{q_{i,m}|\mathbf{w}_m^H\mathbf{h}_{i,m}|^2}{\sum_{j=1}^{2} q_{j,m}|\mathbf{w}_m^H\mathbf{h}_{j,m}|^2} + \frac{q_{i,m}|\mathbf{w}_m^H\mathbf{h}_{i,m}|^2}{\sigma_r^2}\right)\right]^+. \tag{2}$$

C. Downlink Signal Model

For the downlink transmission, the relay uses $\mathbf{w}_m^H\mathbf{Y}_m$ to generate a lattice symbol $\mathbf{s}_m \in \mathbb{C}^{L_m \times 1}$ with power $p_m = \frac{1}{t_m}||\mathbf{s}_m||^2$ (the lattice decoding and encoding procedure at relay can be found in [2, Appendix A]). After the above procedure, the relay transmits $\mathbf{s}_m$ through the transmit beamforming vector $\mathbf{v}_m \in \mathbb{C}^{N \times 1}$ with $||\mathbf{v}_m|| = 1$. Therefore, the received signal $\mathbf{r}_{i,m}^T \in \mathbb{C}^{1 \times L_m}$ at user i is $\mathbf{r}_{i,m}^T = \mathbf{g}_{i,m}^H\mathbf{v}_m\mathbf{s}_m^T + \mathbf{n}_{i,m}^T$, where $\mathbf{g}_{i,m}^H \in \mathbb{C}^{1 \times N}$ is the downlink channel vector from the relay to user i, and $\mathbf{n}_{i,m}^T \in \mathbb{C}^{1 \times L_m}$ is the Gaussian noise at user i with $\mathbb{E}[\mathbf{n}_{i,m}\mathbf{n}_{i,m}^H] = \sigma_u^2\mathbf{I}_{L_m}$. To implement WPT, the received signal at user i in the downlink is further splitted into two branches, one for the information decoder and the other for the energy harvester.

At the information decoder side, the signal is given by $\widetilde{\mathbf{r}}_{i,m}^T = \sqrt{\beta_{i,m}}\mathbf{g}_{i,m}^H\mathbf{v}_m\mathbf{s}_m^T + \sqrt{\beta_{i,m}}\mathbf{n}_{i,m}^T + \mathbf{z}_{i,m}^T$, where $\beta_{i,m}$ is the power splitting factor.[3] and $\mathbf{z}_{i,m}^T \in \mathbb{C}^{1 \times L_m}$ is Gaussian noise introduced by the power splitter, with $\mathbb{E}[\mathbf{z}_{i,m}\mathbf{z}_{i,m}^H] = \sigma_z^2\mathbf{I}_{L_m}$. Based on the expression of $\widetilde{\mathbf{r}}_{i,m}^T$, the downlink SNR for user i is $\beta_{i,m}p_m|\mathbf{g}_{i,m}^H\mathbf{v}_m|^2/(\sigma_u^2\beta_{i,m} + \sigma_z^2)$, and the downlink achievable rate $R_{i,m}^{\text{DL}}$ at user i is expressed as

$$R_{i,m}^{\text{DL}} = \log_2\left(1 + \frac{\beta_{i,m}p_m|\mathbf{g}_{i,m}^H\mathbf{v}_m|^2}{\sigma_u^2\beta_{i,m} + \sigma_z^2}\right). \tag{3}$$

On the other hand, at the energy harvester of user i, the input power can be expressed as $(1 - \beta_{i,m})\mathbb{E}[||\mathbf{r}_{i,m}||^2]/t_m$. Based on the expression of $\mathbf{r}_{i,m}$, it can be further expressed as $(1 - \beta_{i,m})p_m|\mathbf{g}_{i,m}^H\mathbf{v}_m|^2$.

[2]The channels can be pre-determined according to [25].

[3]The considered framework also includes the special case where only one user needs to harvest energy. For example, one user might be a local access point while the other user is a low-cost sensor. In this case, we simply set $\beta_{i,m} = 1$ for the local access point.

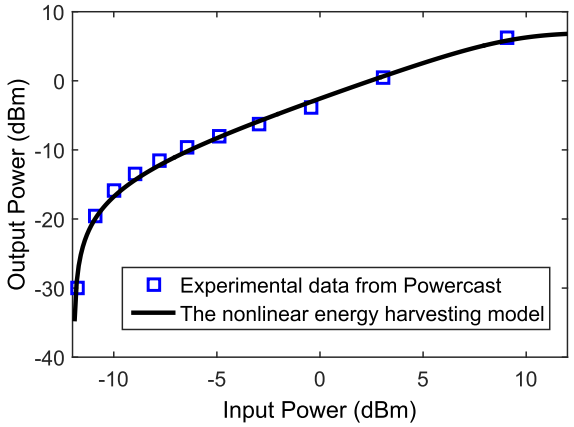

Fig. 2. Comparison between the experimental data and the nonlinear energy harvesting model. The parameters in the model are given by $\tau = 274$, $\nu = 0.29$, $P_{\max} = 0.004927$ W and $P_0 = 0.000064$ W.

D. Energy Harvesting Model

In general, the output power of the energy harvester $P_{\text{out}} = \Theta(P_{\text{in}})$ is a nonlinear function of input power P_{in} [27]–[31], as the energy harvester contains nonlinear elements such as diodes. Particularly, this nonlinear function Θ should satisfy the following properties.

(i) When P_{in} is smaller than the harvester's sensitivity threshold P_0, we must have $P_{\text{out}} = \Theta(P_{\text{in}}) = 0$ [27].
(ii) $\Theta(P_{\text{in}})$ is a monotonically increasing function of P_{in} [28].
(iii) As P_{in} increases, the energy harvesting efficiency $\Theta(P_{\text{in}})/P_{\text{in}}$ would increase to a maximum value and then decrease [29], [30].
(iv) $\Theta(P_{\text{in}}) \leq P_{\max}$ for all P_{in}, where $P_{\max}$ is the maximum harvested power when the energy harvesting circuit is saturated [31].

Based on the properties (ii)-(iv), the function Θ should have an "S" shape, and to capture this shape, a logistic model is proposed in [31]. However, the model in [31] does not satisfy the sensitivity property (i). In order to address the sensitivity issue, we modify the logistic model into the following form:

$$\Theta(P_{\text{in}}) = \left[\frac{P_{\max}}{\exp(-\tau P_0 + \nu)}\left(\frac{1 + \exp(-\tau P_0 + \nu)}{1 + \exp(-\tau P_{\text{in}} + \nu)} - 1\right)\right]^+, \tag{4}$$

and based on (4) the harvested power at user i is $\Theta\left((1 - \beta_{i,m})p_m|\mathbf{g}_{i,m}^H\mathbf{v}_m|^2\right)$. It can be verified that the function Θ in (4) satisfies all the properties (i)-(iv). Moreover, the parameters τ and ν control the steepness of the function Θ.

To evaluate the model in (4), we fit the model to the experimental data from the Powercast energy harvester P2110 [28] at 915 MHz with transmitter-receiver distance ranging from 1 m to 15 m, and the output power versus input power is shown in Fig. 2. It can be observed that the non-linear energy harvesting model in (4) matches the experimental data very well.

III. Achievable Rate Region Problem Formulation

The achievable rate region of TWRC is the set of all achievable rate combinations (R_1, R_2) supported by the system,

where R_i denotes the average data-rate from user i to its paired user. Since the end-to-end transmission consists of uplink and downlink phases, R_i needs to satisfy [19, Th. 1] :

$$R_i \le \frac{1}{T}\sum_{m=1}^{M} t_m \min\left(R_{i,m}^{\mathrm{UL}}, R_{3-i,m}^{\mathrm{DL}}\right), \quad \forall i = 1, 2, \tag{5}$$

where the index $3-i$ is used to represent the paired user of user i due to $i \in \{1, 2\}$.

Having the data-rate constraints satisfied, the users and relay also need to meet their energy requirements. Specifically, as the user transmit power $q_{i,m}$ is harvested from the previous downlink wireless signal, we must have

$$E_i + \sum_{l=1}^{m} t_l \Theta\left((1-\beta_{i,l}) p_l |\mathbf{g}_{i,l}^H \mathbf{v}_l|^2\right) \ge \sum_{l=1}^{m}\left[t_l q_{i,l} + (2t_l + s_l) p_c\right], \quad \forall i = 1, 2,\ m = 1, \ldots, M, \tag{6}$$

where E_i is the initial local energy at user i, and p_c is the users' circuit power consumption. On the other hand, since the energy consumption at relay includes motion energy E_G and transmission energy, we must have

$$E_G + E_c + \sum_{m=1}^{M} t_m p_m \le E_r, \tag{7}$$

where E_r is the energy available for the relay to use and E_c is the circuit energy consumption at relay. Finally, the variables $\{t_m, \mathbf{v}_m, \mathbf{w}_m, p_m, q_{i,m}, \beta_{i,m}\}$ need to satisfy the following basic constraints

$$\begin{aligned} &\sum_{m=1}^{M}(2t_m + s_m) = T, \\ &\quad t_m \ge 0, \quad ||\mathbf{v}_m|| = ||\mathbf{w}_m|| = 1, \ \ p_m \ge 0, m = 1, \ldots, M \\ &\quad q_{i,m} \ge 0, \quad \beta_{i,m} \in [0, 1], \ \ i = 1, 2, \ \ m = 1, \ldots, M. \end{aligned} \tag{8}$$

Under the constraints (5)-(8), the achievable rate region $\mathcal{R}(\mathbf{e}, \mathcal{H})$ is defined as a function of node energies $\mathbf{e} := [E_r, E_1, E_2]$ and user channels along the trajectory $\mathcal{H} := \{\mathbf{h}_{i,m}, \mathbf{g}_{i,m}, \ i = 1, 2, \ m = 1, \ldots, M\}$:

$$\mathcal{R}(\mathbf{e}, \mathcal{H}) = \left\{(R_1, R_2) \in \mathbb{R}_+^2 : (5) - (8)\right\}.$$

Because $\mathcal{R}(\mathbf{e}, \mathcal{H})$ is a solid region, determining this region means determining its boundary. That is, finding the Pareto optimal solutions that maximize the data-rate pair (R_1, R_2) [32]. However, since R_1 and R_2 are interdependent, the vector (R_1, R_2) can be transformed into $(\mu_1 R_{\mathrm{sum}}, \mu_2 R_{\mathrm{sum}})$, where $R_{\mathrm{sum}} := R_1 + R_2$ and $\mu_i := R_i / R_{\mathrm{sum}}$ satisfying $\mu_1 + \mu_2 = 1$ [17, Sec. III-B]. After this transformation, a point on the rate region boundary can be obtained as $(\mu_1 R_{\mathrm{sum}}^*, \mu_2 R_{\mathrm{sum}}^*)$, where R_{sum}^* is the maximum sum-rate by solving the following problem with a given μ_1:

$$\begin{aligned} \mathrm{P1}: \max_{R_{\mathrm{sum}}, \{t_m, \mathbf{v}_m, \mathbf{w}_m, p_m, q_{i,m}, \beta_{i,m}\}} \ & R_{\mathrm{sum}} \\ \text{s.t. } & \frac{1}{T}\sum_{m=1}^{M} \min\left\{ t_m\left[\log_2\left(\frac{q_{i,m}|\mathbf{w}_m^H \mathbf{h}_{i,m}|^2}{\sum_{j=1}^{2} q_{j,m}|\mathbf{w}_m^H \mathbf{h}_{j,m}|^2} + \frac{q_{i,m}|\mathbf{w}_m^H \mathbf{h}_{i,m}|^2}{\sigma_r^2}\right)\right]^+, \right. \\ & \left. t_m \log_2\left(1 + \frac{\beta_{3-i,m} p_m |\mathbf{g}_{3-i,m}^H \mathbf{v}_m|^2}{\sigma_u^2 \beta_{3-i,m} + \sigma_z^2}\right)\right\} \\ & \ge \mu_i R_{\mathrm{sum}}, \quad \forall i = 1, 2 \qquad (9a) \\ & E_i + \sum_{l=1}^{m} t_l \Theta\left((1-\beta_{i,l}) p_l |\mathbf{g}_{i,l}^H \mathbf{v}_l|^2\right) \\ & \ge \sum_{l=1}^{m}\left[t_l q_{i,l} + (2t_l + s_l) p_c\right], \\ & \forall i = 1, 2, \quad m = 1, \ldots, M \qquad (9b) \\ & E_G + E_c + \sum_{m=1}^{M} t_m p_m \le E_r, \\ & \sum_{m=1}^{M}(2t_m + s_m) = T \qquad (9c) \\ & t_m \ge 0, \quad p_m \ge 0, \ ||\mathbf{v}_m|| = ||\mathbf{w}_m|| = 1, \\ & \forall m = 1, \ldots, M \qquad (9d) \\ & \beta_{i,m} \in [0, 1], \quad q_{i,m} \ge 0, \\ & \forall i = 1, 2, \quad m = 1, \ldots, M. \qquad (9e) \end{aligned}$$

Then by varying μ_1 within the interval $(0, 1)$ and solving P1 repeatedly, we can obtain a set of boundary points and thus the achievable rate region $\mathcal{R}(\mathbf{e}, \mathcal{H})$.

IV. Exact Achievable Rate Region for Fixed Relay Case

To solve P1, we first consider its special case of $M = 1$, i.e., wirelessly powered TWRC with a fixed relay. This special case is very important for analyzing the performance gain brought by energy harvesting and for subsequent comparison with the general case of mobile relay. In particular, since the trajectory length is zero when $M = 1$, we have $s_1 = 0$ and $E_G = 0$, and the constraint $\sum_{m=1}^{M}(2t_m + s_m) = T$ reduces to $2t_1 = T$. Furthermore, due to $M = 1$, the subscript m can be dropped to simplify the notation. Therefore, problem P1 becomes

$$\begin{aligned} \mathrm{F1}: \max_{R_{\mathrm{sum}}, \mathbf{v}, \mathbf{w}, p, \{q_i, \beta_i\}} \ & R_{\mathrm{sum}} \\ \text{s.t. } & \left[\log_2\left(\frac{q_i |\mathbf{w}^H \mathbf{h}_i|^2}{\sum_{j=1}^{2} q_j |\mathbf{w}^H \mathbf{h}_j|^2} + \frac{q_i |\mathbf{w}^H \mathbf{h}_i|^2}{\sigma_r^2}\right)\right]^+ \\ & \ge 2\mu_i R_{\mathrm{sum}}, \quad \forall i \\ & \log_2\left(1 + \frac{\beta_i p |\mathbf{g}_i^H \mathbf{v}|^2}{\sigma_u^2 \beta_i + \sigma_z^2}\right) \ge 2\mu_{3-i} R_{\mathrm{sum}}, \quad \forall i \\ & \frac{2E_i}{T} + \Theta\left((1-\beta_i) p |\mathbf{g}_i^H \mathbf{v}|^2\right) \ge q_i + 2p_c, \quad \forall i \\ & q_i \ge 0, \quad \beta_i \in [0, 1], \ \forall i, \ p \in \left[0, \frac{2E_r - 2E_c}{T}\right], \\ & ||\mathbf{v}|| = 1, \quad ||\mathbf{w}|| = 1. \end{aligned}$$

A. Recasting F1 as a Feasibility Problem

Given a fixed μ_1 (and thus fixed μ_2), a simple way to determine R^*_{sum} in F1 is to increase R_{sum} from 0 until the problem becomes infeasible, where the feasibility of F1 with a fixed R_{sum} is discussed in the next paragraph. On the other hand, a more efficient way to search for R^*_{sum} is to use bisection algorithm. Specifically, given an upper bound for the searching interval, say $\kappa_{\max}$, and a lower bound $\kappa_{\min}$, the trial point is set to $\kappa = (\kappa_{\max} + \kappa_{\min})/2$. If F1 with $R_{\text{sum}} = \kappa$ is feasible, the lower bound is updated as $\kappa_{\min} = \kappa$; otherwise, the upper bound is updated as $\kappa_{\max} = \kappa$. The process is repeated until $|\kappa_{\max} - \kappa| < \epsilon$, where ϵ is a small positive constant to control the accuracy. As $R_{\text{sum}} \geq 0$, an initial $\kappa_{\min}$ can be chosen as 0. On the other hand, a valid initial $\kappa_{\max}$ can be found as follows. From the second line of constraints of F1, we have

$$R_{\text{sum}} \leq \frac{1}{2}\min\left[\log_2\left(1+\frac{\beta_1 p|\mathbf{g}_1^H\mathbf{v}|^2}{\sigma_u^2\beta_1+\sigma_z^2}\right)/\mu_2,\right. \\ \left.\log_2\left(1+\frac{\beta_2 p|\mathbf{g}_2^H\mathbf{v}|^2}{\sigma_u^2\beta_2+\sigma_z^2}\right)/\mu_1\right]. \quad (10)$$

Using the constraints in the last line of F1, it can be observed that $\log_2(1+\frac{\beta_i p|\mathbf{g}_i^H\mathbf{v}|^2}{\sigma_u^2\beta_i+\sigma_z^2})$ is maximized when $\mathbf{v} = \mathbf{g}_i/||\mathbf{g}_i||$, $p = (2E_r - 2E_c)/T$ and $\beta_i = 1$. Therefore, a valid upper bound of R_{sum} is given by

$$R_{\text{sum}} \leq \frac{1}{2}\min\left[\log_2\left(1+\frac{(2E_r-2E_c)||\mathbf{g}_1||^2}{T(\sigma_u^2+\sigma_z^2)}\right)/\mu_2,\right. \\ \left.\log_2\left(1+\frac{(2E_r-2E_c)||\mathbf{g}_2||^2}{T(\sigma_u^2+\sigma_z^2)}\right)/\mu_1\right]. \quad (11)$$

With the obtained upper bound, we are now ready to apply the bisection algorithm to find R^*_{sum} in F1. An efficient way to provide a feasibility check of F1 given $R_{\text{sum}} = \kappa$ is to first minimize the transmit power p via the following problem

$$\text{F2}: \min_{\mathbf{v},\mathbf{w},p\geq 0,\{q_i\geq 0,\beta_i\}} \quad p \quad (12a)$$

$$\text{s.t.} \quad \frac{q_i|\mathbf{w}^H\mathbf{h}_i|^2}{\sum_{j=1}^2 q_j|\mathbf{w}^H\mathbf{h}_j|^2} + \frac{q_i|\mathbf{w}^H\mathbf{h}_i|^2}{\sigma_r^2} \geq 2^{2\mu_i\kappa}, \quad \forall i \quad (12b)$$

$$1+\frac{\beta_i p|\mathbf{g}_i^H\mathbf{v}|^2}{\sigma_u^2\beta_i+\sigma_z^2} \geq 2^{2\mu_{3-i}\kappa}, \quad \forall i \quad (12c)$$

$$\Theta\Big((1-\beta_i)p|\mathbf{g}_i^H\mathbf{v}|^2\Big) + \frac{2E_i}{T} \geq q_i + 2p_c, \quad \forall i \quad (12d)$$

$$\beta_i \in [0,1], \quad \forall i,\ ||\mathbf{v}|| = 1,\ ||\mathbf{w}|| = 1, \quad (12e)$$

and then check whether the optimal p^* satisfies $p^* \leq (2E_r - 2E_c)/T$. If so, problem F1 with $R_{\text{sum}} = \kappa$ is feasible; otherwise, the transmit power or energy at relay cannot support sum-rate κ and F1 with $R_{\text{sum}} = \kappa$ is infeasible. Notice that (12b) comes from the first constraint of F1 with the operator $[\cdot]^+$ dropped. However, dropping the operator would not change the constraint due to $2^{2\mu_i\kappa} \geq 1$. On the other hand, the constraint (12c) comes from the second constraint of F1.

B. Dimension Reduction

Since F2 is a high dimensional problem, we will first reduce its dimension based on the following procedure. More specifically, applying [2, Property 1] to the first constraint (12b) and defining $\alpha_i = 2^{2\mu_i\kappa} - 2^{2\mu_i\kappa}/(2^{2\mu_1\kappa} + 2^{2\mu_2\kappa})$, it can be shown that (12b) could be replaced by $q_i = \alpha_i\sigma_r^2/|\mathbf{w}^H\mathbf{h}_i|^2$ without changing the optimal objective value of F2. Putting this result into (12d), constraint (12d) is equivalent to

$$\Theta\Big((1-\beta_i)|\mathbf{g}_i^H\mathbf{v}|^2 p\Big) \geq \frac{\alpha_i\sigma_r^2}{|\mathbf{w}^H\mathbf{h}_i|^2} + 2p_c - \frac{2E_i}{T}, \quad \forall i. \quad (13)$$

On the other hand, constraint (12c) can be reformulated as

$$\beta_i|\mathbf{g}_i^H\mathbf{v}|^2 p \geq \theta_i(\sigma_u^2\beta_i + \sigma_z^2), \quad \forall i, \quad (14)$$

with $\theta_i = 2^{2\mu_{3-i}\kappa} - 1$. Based on the above manipulations, problem F2 is equivalently transformed into

$$\min_{p,\mathbf{v},\mathbf{w},\{\beta_i\}} \quad p \quad (15)$$
$$\text{s.t. (13), (14)}$$
$$\beta_i \in [0,1], \quad \forall i,\ ||\mathbf{v}|| = 1,\ ||\mathbf{w}|| = 1.$$

To reduce the dimension of problem (15), we apply [2, Property 2] to obtain the optimal $\mathbf{w}^* \in \text{span}\{\mathbf{h}_1, \mathbf{h}_2\}$. Moreover, due to property (ii) of $\Theta(x)$ and by using [2, Property 2], the optimal $\mathbf{v}^* \in \text{span}\{\mathbf{g}_1, \mathbf{g}_2\}$. Therefore, the Schmidt orthogonal basis for $\mathbf{v}^*$ is given by $\mathbf{g}_1$ and $\mathbf{z} = \mathbf{g}_2 - \mathbf{g}_1^H\mathbf{g}_2/||\mathbf{g}_1||^2\cdot\mathbf{g}_1$. Using this basis and the norm constraint of $\mathbf{v}$, we can express the transmit beamformer $\mathbf{v}$ as

$$\mathbf{v}(\rho,\phi_1,\phi_2) = \sqrt{\rho}\cdot\exp(\text{j}\phi_1)\frac{\mathbf{g}_1}{||\mathbf{g}_1||} + \sqrt{1-\rho}\cdot\exp(\text{j}\phi_2)\frac{\mathbf{z}}{||\mathbf{z}||}, \quad (16)$$

where the scalar variable $0 \leq \rho \leq 1$ and $\text{j} = \sqrt{-1}$. To determine ϕ_1 and ϕ_2, we first compute $|\mathbf{g}_1^H\mathbf{v}| = \sqrt{\rho}||\mathbf{g}_1||$ and $|\mathbf{g}_2^H\mathbf{v}| = \left|\sqrt{\rho}\text{e}^{\text{j}\phi_1}\mathbf{g}_2^H\mathbf{g}_1/||\mathbf{g}_1|| + \sqrt{1-\rho}\text{e}^{\text{j}\phi_2}||\mathbf{z}||\right|$ using (16). Then according to [33, Lemma 5–6], we have $\phi_2 - \phi_1 = \angle(\mathbf{g}_2^H\mathbf{g}_1)$. As a common phase between ϕ_1 and ϕ_2 does not affect $|\mathbf{g}_i^H\mathbf{v}|$, without loss of generality, we set $\phi_1 = 0$. Putting this result into (16), we obtain

$$\mathbf{v}(\rho) = \sqrt{\rho}\cdot\frac{\mathbf{g}_1}{||\mathbf{g}_1||} + \sqrt{1-\rho}\cdot\exp[\text{j}\angle(\mathbf{g}_2^H\mathbf{g}_1)]\frac{\mathbf{z}}{||\mathbf{z}||}. \quad (17)$$

With a similar procedure to $\mathbf{v}$, it can be shown that the receive beamformer $\mathbf{w}$ can be expressed as

$$\mathbf{w}(\gamma) = \sqrt{\gamma}\cdot\frac{\mathbf{h}_1}{||\mathbf{h}_1||} + \sqrt{1-\gamma}\cdot\exp[\text{j}\angle(\mathbf{h}_2^H\mathbf{h}_1)]\frac{\mathbf{u}}{||\mathbf{u}||}, \quad (18)$$

where the scalar variable $0 \leq \gamma \leq 1$, and $\mathbf{u} = \mathbf{h}_2 - \mathbf{h}_1^H\mathbf{h}_2/||\mathbf{h}_1||^2\cdot\mathbf{h}_1$. By putting (17) and (18) into problem (15), the following equivalent problem is obtained

$$\text{F3}: \min_{p,\rho,\gamma,\{\beta_i\}} \quad p$$
$$\text{s.t.} \ (1-\beta_i)A_i(\rho)p \geq B_i(\gamma), \quad \forall i = 1,2 \quad (19a)$$
$$\beta_i A_i(\rho)p \geq \theta_i(\sigma_u^2\beta_i + \sigma_z^2), \quad \forall i = 1,2 \quad (19b)$$
$$\rho \in [0,1], \quad \gamma \in [0,1], \ \beta_i \in [0,1], \ \forall i = 1,2, \quad (19c)$$

where

$$A_1(\rho) = \rho||\mathbf{g}_1||^2, \quad A_2(\rho) = \left(\sqrt{\rho}\frac{|\mathbf{g}_2^H\mathbf{g}_1|}{||\mathbf{g}_1||} + \sqrt{1-\rho}||\mathbf{z}||\right)^2$$

$$B_1(\gamma) = \Theta^\dagger\left(\frac{\alpha_1\sigma_r^2}{\gamma||\mathbf{h}_1||^2} + 2p_c - \frac{2E_1}{T}\right)$$

$$B_2(\gamma) = \Theta^\dagger\left(\frac{\alpha_2\sigma_r^2}{(\sqrt{\gamma}\frac{|\mathbf{h}_2^H\mathbf{h}_1|}{||\mathbf{h}_1||} + \sqrt{1-\gamma}||\mathbf{u}||)^2} + 2p_c - \frac{2E_2}{T}\right)$$

$$\Theta^\dagger(x) = \begin{cases} +\infty, & \text{if } x \geq P_{\max} \\ \frac{\nu}{\tau} - \frac{1}{\tau}\ln\Big(\frac{1+\exp(-\tau P_0+\nu)}{1+P_{\max}^{-1}\exp(-\tau P_0+\nu)x} \\ \quad -1\Big), & \text{if } 0 < x < P_{\max} \\ 0, & \text{if } x \leq 0. \end{cases} \tag{20}$$

Now, problem F3 only has four independent scalar variables, and is of much lower dimension than problem (15). A naive way to solve F3 is to perform a four-dimensional exhaustive search over ρ, γ, β_1 and β_2. However, this approach has a very high computational complexity. Below, we will show that F3 has a closed-form solution for a fixed γ. Therefore, F3 can be reduced to a one-dimensional search problem over γ.

C. Closed-Form Solution of F3 Given γ

In this subsection, we derive the solution $\{p^\diamond, \rho^\diamond, \beta_i^\diamond\}$ of F3 given a fixed γ. To simplify the notation, variables that are functions of γ only are written as constants, e.g., $B_i(\gamma)$ is written as B_i. To begin with, we will determine the optimal solution of β_1 and β_2. Since the constraints (19a) may be redundant depending on the values of B_1 and B_2, we divide the discussion into two cases below.

(i) If $B_i = 0$, then (19a) will always be satisfied. Furthermore, the constraint (19b) can be rewritten as $p \geq \frac{\theta_i}{A_i(\rho)}(\sigma_u^2 + \frac{\sigma_z^2}{\beta_i})$. From this equivalent constraint, the feasibility space of p is enlarged by using the maximum value of β_i in [0, 1] [34]. This gives $\beta_i = 1$.

(ii) If $B_i > 0$, from (19a) we immediately have $\beta_i = 1$ is not feasible. On the other hand, due to $\theta_i = 2^{2\mu_{3-i}\kappa} - 1$ defined under (14) and $\mu_{3-i} > 0$, we must have $\theta_i > 0$ and therefore from (19b) $\beta_i \neq 0$. Then, the range of β_i becomes (0, 1), and (19a) and (19b) can be rewritten as $p \geq \frac{B_i}{(1-\beta_i)A_i(\rho)}$ and $p \geq \frac{\theta_i}{A_i(\rho)}(\sigma_u^2 + \frac{\sigma_z^2}{\beta_i})$, respectively. Taking the intersection of the above inequalities, they can be combined as

$$p \geq \max\left(\frac{B_i}{(1-\beta_i)A_i(\rho)}, \frac{\theta_i}{A_i(\rho)}\left(\sigma_u^2 + \frac{\sigma_z^2}{\beta_i}\right)\right). \tag{21}$$

Inside the max function of (21), the first term is an increasing function of β_i while the second term is a decreasing function of β_i. Therefore, the minimum of p is obtained when

$$\frac{B_i}{(1-\beta_i)A_i(\rho)} = \frac{\theta_i}{A_i(\rho)}\left(\sigma_u^2 + \frac{\sigma_z^2}{\beta_i}\right). \tag{22}$$

Solving (22) for β_i leads to

$$\beta_i^\diamond = \frac{2\sigma_z^2}{\sigma_z^2 - \sigma_u^2 + \frac{B_i}{\theta_i} + \sqrt{\left(\sigma_z^2 - \sigma_u^2 + \frac{B_i}{\theta_i}\right)^2 + 4\sigma_u^2\sigma_z^2}}. \tag{23}$$

Combining the two cases above, we have the following result.

Property 1: The optimal $\beta_i^\diamond$ to F3 *with γ fixed is given by* (23) *when $B_i > 0$; otherwise $\beta_i^\diamond = 1$.*

Putting the result of **Property 1** into the constraints (19a) and (19b), they can be combined into $p \geq \frac{\xi_i}{A_i(\rho)}$ for $i = 1, 2$, where

$$\xi_i = \begin{cases} \frac{\theta_i}{2}\Big(\sigma_z^2 + \sigma_u^2 + \frac{B_i}{\theta_i} \\ \quad + \sqrt{\left(\sigma_z^2 - \sigma_u^2 + \frac{B_i}{\theta_i}\right)^2 + 4\sigma_u^2\sigma_z^2}\Big), & \text{if } B_i > 0 \\ \theta_i(\sigma_u^2 + \sigma_z^2), & \text{if } B_i = 0. \end{cases} \tag{24}$$

By further taking the intersection of both users' constraints, (19a) and (19b) become $p \geq \max(\frac{\xi_1}{A_1(\rho)}, \frac{\xi_2}{A_2(\rho)})$. As a result, F3 with a fixed γ is reduced into

$$\text{F4}: \min_{p,\rho\in[0,1]} \left\{p : p \geq \max\left(\frac{\xi_1}{A_1(\rho)}, \frac{\xi_2}{A_2(\rho)}\right)\right\}. \tag{25}$$

With the definition of $A_1(\rho)$ in (20), it is clear that the term $\frac{\xi_1}{A_1(\rho)}$ in (25) is a decreasing function of ρ, and its minimum is obtained when $\rho = 1$. On the other hand, taking the derivative of $\frac{\xi_2}{A_2(\rho)}$ with respect to ρ, we have

$$\frac{\partial\left(\xi_2/A_2(\rho)\right)}{\partial\rho} = -2\xi_2\left(\sqrt{\rho}\frac{|\mathbf{g}_2^H\mathbf{g}_1|}{||\mathbf{g}_1||} + \sqrt{1-\rho}||\mathbf{z}||\right)^{-3} \times \left(\frac{1}{2\sqrt{\rho}}\frac{|\mathbf{g}_2^H\mathbf{g}_1|}{||\mathbf{g}_1||} - \frac{1}{2\sqrt{1-\rho}}||\mathbf{z}||\right). \tag{26}$$

Setting $\frac{\partial\left(\xi_2/A_2(\rho)\right)}{\partial\rho} = 0$, we get $\rho = \frac{|\mathbf{g}_2^H\mathbf{g}_1|^2}{||\mathbf{g}_1||^2||\mathbf{g}_2||^2}$. Notice that when $\rho < \frac{|\mathbf{g}_2^H\mathbf{g}_1|^2}{||\mathbf{g}_1||^2||\mathbf{g}_2||^2}$, we have $\frac{\partial\left(\xi_2/A_2(\rho)\right)}{\partial\rho} < 0$, and when $\rho > \frac{|\mathbf{g}_2^H\mathbf{g}_1|^2}{||\mathbf{g}_1||^2||\mathbf{g}_2||^2}$, we have $\frac{\partial\left(\xi_2/A_2(\rho)\right)}{\partial\rho} > 0$. As a result, $\rho = \frac{|\mathbf{g}_2^H\mathbf{g}_1|^2}{||\mathbf{g}_1||^2||\mathbf{g}_2||^2}$ is the minimum point of $\frac{\xi_2}{A_2(\rho)}$.

Based on the above analysis, we can plot the two functions $\frac{\xi_1}{A_1(\rho)}$ and $\frac{\xi_2}{A_2(\rho)}$ as in Fig. 3. It is observed from Fig. 3 that there are three possibilities for $\min_{\rho\in[0,1]}\max\left(\frac{\xi_1}{A_1(\rho)}, \frac{\xi_2}{A_2(\rho)}\right)$, and the optimal $\rho^\diamond$ must be within the set

$$\mathcal{G} = \left\{1, \frac{|\mathbf{g}_2^H\mathbf{g}_1|^2}{||\mathbf{g}_1||^2||\mathbf{g}_2||^2}, \rho^{\text{int}}\right\}, \tag{27}$$

where ρ^{int} is the intersection point of $\frac{\xi_1}{A_1(\rho)}$ and $\frac{\xi_2}{A_2(\rho)}$, which can be calculated using $\frac{\xi_1}{A_1(\rho)} = \frac{\xi_2}{A_2(\rho)}$,

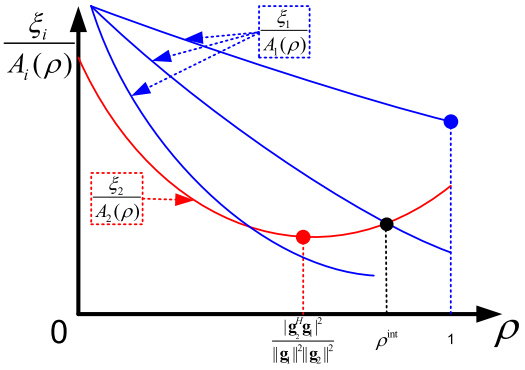

Fig. 3. Illustration of $\frac{\xi_1}{A_1(\rho)}$ and $\frac{\xi_2}{A_2(\rho)}$.

i.e., $\xi_1\left(\sqrt{\rho}\frac{|\mathbf{g}_2^H\mathbf{g}_1|}{\|\mathbf{g}_1\|}+\sqrt{1-\rho}\|\mathbf{z}\|\right)^2 = \xi_2\rho\|\mathbf{g}_1\|^2$. Taking square root on both sides gives

$$\rho^{\text{int}}=\frac{\xi_1\|\mathbf{z}\|^2}{\left(\sqrt{\xi_2}\|\mathbf{g}_1\|-\sqrt{\xi_1}\frac{|\mathbf{g}_2^H\mathbf{g}_1|}{\|\mathbf{g}_1\|}\right)^2+\xi_1\|\mathbf{z}\|^2}. \quad (28)$$

With the optimal $\rho^\diamond$ being in the set $\mathcal{G}$ and since p is a variable to be minimized, the optimal $p^\diamond$ to problem F4 (thus to problem F3 with γ fixed) is given by

$$p^\diamond=\min_{\rho\in\mathcal{G}}\ \max\left(\frac{\xi_1}{A_1(\rho)},\frac{\xi_2}{A_2(\rho)}\right). \quad (29)$$

In conclusion, the procedure for computing the achievable rate region when $M=1$ is summarized in Algorithm 1.

Algorithm 1 Computing the Achievable Rate Region $\mathcal{R}(\mathbf{e},\mathcal{H})$ With Fixed Relay Position

1: **Given** $\mathbf{e}$, $\mathcal{H}$ and parameters T, p_c, μ_1.
2: **Initialize** $\kappa_{\max}$ using (11) and $\kappa_{\min}=0$.
3: **Repeat**
4: Update $\kappa=(\kappa_{\min}+\kappa_{\max})/2$.
5: Solve $p^*=\min_{\gamma\in[0,1]}\ p^\diamond(\gamma)$, where $p^\diamond(\gamma)$ is obtained from (29).
6: Update $\kappa_{\min}=\kappa$ if $p^*\le(2E_r-2E_c)/T$; $\kappa_{\max}=\kappa$ if $p^*>(2E_r-2E_c)/T$.
7: **Until** $|\kappa_{\max}-\kappa|<\epsilon$, where ϵ is a small positive constant to control the accuracy.
8: Set $R_{\text{sum}}^*=\kappa$, and a point on the boundary of achievable rate region is given by $(\mu_1R_{\text{sum}}^*,\mu_2R_{\text{sum}}^*)$.
9: **Vary** μ_1 from 0 to 1 and repeat the above steps.

V. Rate Region Bounds for Mobile Relay Case

In order to analyze the performance gain brought by the moving relay, in this section, we consider the case of $M\ge2$ for which the relay is moving along a pre-defined trajectory and has multiple stopping points. While exactly solving P1 in such a case is generally difficult, we can derive a pair of tight inner and outer bounds to locate the achievable rate region.

To derive the inner and outer bounds, the first challenge is to resolve the nonlinear coupling between the stopping time $\{t_m\}$ and the variables $\{\mathbf{w}_m,q_{i,m},\mathbf{v}_m,p_m,\beta_{i,m}\}$ in the logarithm of data-rates, which is apparent in the first constraint of P1. To this end, we introduce substitution variables $\{Q_{i,m},\mathbf{V}_m,\omega_{i,m}\}$ to replace $\{q_{i,m},p_m,\mathbf{v}_m,\beta_{i,m}\}$ as

$$q_{i,m}=\frac{Q_{i,m}}{t_m}\cdot\frac{1}{|\mathbf{w}_m^H\mathbf{h}_{i,m}|^2},\quad \forall i=1,2,\ m=1,\ldots,M,$$
$$p_m\mathbf{v}_m\mathbf{v}_m^H=\frac{\mathbf{V}_m}{t_m}\succeq0,\quad \text{Rank}(\mathbf{V}_m)\le1,\ \forall m=1,\ldots,M,$$
$$\beta_{i,m}=\omega_{i,m}\cdot\frac{1}{\text{Tr}(\mathbf{g}_{i,m}\mathbf{g}_{i,m}^H\mathbf{V}_m)},\quad \forall i=1,2,\ m=1,\ldots,M.$$

Based on the above variable substitution, the constraint (9a) of P1 is rewritten as

$$\frac{1}{T}\sum_{m=1}^{M}\min\left\{t_m\left[\log_2\left(\frac{Q_{i,m}}{Q_{1,m}+Q_{2,m}}+\frac{Q_{i,m}}{\sigma_r^2t_m}\right)\right]^+,\ t_m\log_2\left(1+\frac{\beta_{3-i,m}\text{Tr}(\mathbf{g}_{3-i,m}\mathbf{g}_{3-i,m}^H\mathbf{V}_m)}{(\beta_{3-i,m}\sigma_u^2+\sigma_z^2)t_m}\right)\right\}\ge\mu_iR_{\text{sum}},$$

which can be further reformulated as

$$\frac{1}{T}\sum_{m=1}^{M}\min\left\{\left[t_m\log_2\left(\frac{Q_{i,m}}{\sigma_r^2t_m}\right)+t_m\log_2\left(1+\frac{\sigma_r^2t_m}{Q_{1,m}+Q_{2,m}}\right)\right]^+,\ t_m\log_2\left(1+\frac{1}{(\frac{\sigma_u^2}{\text{Tr}(\mathbf{g}_{3-i,m}\mathbf{g}_{3-i,m}^H\mathbf{V}_m)}+\frac{\sigma_z^2}{\omega_{3-i,m}})t_m}\right)\right\}\ge\mu_iR_{\text{sum}}, \quad (30)$$

where the first line of (30) is obtained by using $\frac{Q_{i,m}}{Q_{1,m}+Q_{2,m}}+\frac{Q_{i,m}/t_m}{\sigma_r^2}=\frac{Q_{i,m}/t_m}{\sigma_r^2}\cdot\left(1+\frac{\sigma_r^2t_m}{Q_{1,m}+Q_{2,m}}\right)$, while the second line of (30) is obtained by dividing the numerator and the denominator of $\frac{\beta_{3-i,m}\text{Tr}(\mathbf{g}_{3-i,m}\mathbf{g}_{3-i,m}^H\mathbf{V}_m)}{(\beta_{3-i,m}\sigma_u^2+\sigma_z^2)t_m}$ by $\beta_{3-i,m}\text{Tr}(\mathbf{g}_{3-i,m}\mathbf{g}_{3-i,m}^H\mathbf{V}_m)$. With further introduction of slack variables $\{a_{i,m}:\frac{1}{a_{i,m}}=\frac{\sigma_u^2}{\text{Tr}(\mathbf{g}_{i,m}\mathbf{g}_{i,m}^H\mathbf{V}_m)}+\frac{\sigma_z^2}{\omega_{i,m}}\}$ and $\{r_{i,m}:r_{i,m}=\min\left(\left[t_m\log_2(\frac{Q_{i,m}}{\sigma_r^2t_m})+t_m\log_2\left(1+\frac{\sigma_r^2t_m}{Q_{1,m}+Q_{2,m}}\right)\right]^+,t_m\log_2(1+\frac{a_{i,m}}{t_m})\right)\}$ for the constraint (30), the constraint (30) can be significantly simplified. Moreover, since the newly added equalities can be relaxed into inequality constraints and such a relaxation would not change the problem (as the optimal slack variables always activate the inequalities), problem P1 can be equivalently reformulated as

$$\text{P2}:\ \max_{R_{\text{sum}},\{t_m,\mathbf{V}_m,\mathbf{w}_m,Q_{i,m},\varphi_{i,m}\},\{r_{i,m},a_{i,m},b_{i,m},c_{i,m}\}}\ R_{\text{sum}}$$
$$\text{s.t. } \mu_iR_{\text{sum}}-\frac{1}{T}\sum_{m=1}^{M}r_{i,m}\le0,\quad\forall i \quad (31a)$$
$$r_{i,m}+\left[-t_m\log_2\left(\frac{Q_{i,m}}{\sigma_r^2t_m}\right)-t_m\log_2\left(1+\frac{\sigma_r^2t_m}{Q_{1,m}+Q_{2,m}}\right)\right]^-\le0,\quad\forall i,m \quad (31b)$$
$$r_{3-i,m}-t_m\log_2\left(1+\frac{a_{i,m}}{t_m}\right)\le0,\quad\forall i,m \quad (31c)$$
$$\frac{\sigma_u^2}{\text{Tr}(\mathbf{g}_{i,m}\mathbf{g}_{i,m}^H\mathbf{V}_m)}+\frac{\sigma_z^2}{\omega_{i,m}}-\frac{1}{a_{i,m}}\le0,\quad\forall i,m \quad (31d)$$

$$\sum_{l=1}^{m}\left[b_{i,l}-t_l\Theta\left(\frac{1}{\tau}\ln\left(\frac{c_{i,l}}{t_l}\right)\right)+(2t_l+s_l)p_c\right]\le E_i,\quad \forall i,m \tag{31e}$$

$$\frac{1}{b_{i,m}}-\frac{|\mathbf{w}_m^H\mathbf{h}_{i,m}|^2}{Q_{i,m}}\le 0,\quad \forall i,m \tag{31f}$$

$$\mathrm{Tr}(\mathbf{g}_{i,m}\mathbf{g}_{i,m}^H\mathbf{V}_m)-\omega_{i,m}\ge\frac{t_m}{\tau}\ln\left(\frac{c_{i,m}}{t_m}\right),\quad \forall i,m \tag{31g}$$

$$E_G+E_c+\sum_{m=1}^{M}\mathrm{Tr}(\mathbf{V}_m)\le E_r,\ \sum_{m=1}^{M}(2t_m+s_m)=T \tag{31h}$$

$$t_m\ge 0,\quad \mathbf{V}_m\succeq 0,\ ||\mathbf{w}_m||\le 1,\quad \forall m \tag{31i}$$

$$Q_{i,m}\ge 0,\quad \omega_{i,m}\ge 0,\ c_{i,m}\ge t_m\quad \forall i,m \tag{31j}$$

$$\mathrm{Rank}(\mathbf{V}_m)\le 1,\quad \forall m. \tag{31k}$$

Notice that the constraint (30) becomes (31a)-(31d), while (31e)-(31g) come from the constraint (9b) of P1 by introducing slack variables $\{b_{i,m}:\frac{Q_{i,m}}{|\mathbf{w}_m^H\mathbf{h}_{i,m}|^2}\le b_{i,m}\}$ and $\{c_{i,m}:\frac{\mathrm{Tr}(\mathbf{g}_{i,m}\mathbf{g}_{i,m}^H\mathbf{V}_m)-\omega_{i,m}}{t_m}\ge\frac{1}{\tau}\ln(\frac{c_{i,m}}{t_m})\}$. Furthermore, the constraints (9c)-(9e) of P1 become (31h)-(31k) and the constraint $||\mathbf{w}_m||=1$ is relaxed into $||\mathbf{w}_m||\le 1$ which would not change the problem due to the optimal $||\mathbf{w}_m^*||=1$.

To proceed to solve P2, the second challenge is the rank constraints in (31k). To this end, we will apply the rank relaxation to drop the rank constraints [35], and a property (proved in Appendix A) can be established to show that the relaxation does not affect the optimality.

Property 2: The rank relaxed problem of P2 *has at least one optimal solution* $\mathbf{V}_m^*$ *with* $\mathrm{Rank}(\mathbf{V}_m^*)\le 1$.

Property 2 guarantees that an optimal rank-one or rank-zero solution to the rank relaxed problem of P2 exists. However, there may be an alternative solution with a higher rank. If we obtain such a solution, the rank reduction procedure in [36] can be applied to obtain the rank-one solution. Therefore, the problem P2 is equivalent to its rank relaxed problem, and we shall focus on the rank relaxed problem in the subsequent part.

A. Inner Bound

With the rank constraints being relaxed, the next challenge in P2 comes from the operator $[\cdot]^-$ in (31b) and the nonlinear function $-t_l\Theta\left(\frac{1}{\tau}\ln(\frac{c_{i,l}}{t_l})\right)$ in (31e). However, based on the expression of Θ in (4), $-t_l\Theta\left(\frac{1}{\tau}\ln(\frac{c_{i,l}}{t_l})\right)$ in (31e) can be expanded as

$$\begin{aligned}&-t_l\Theta\left(\frac{1}{\tau}\ln\left(\frac{c_{i,l}}{t_l}\right)\right)\\&=-t_l\left[\frac{P_{\max}}{\exp(-\tau P_0+\nu)}\left(\frac{1+\exp(-\tau P_0+\nu)}{1+\exp(\nu)(\frac{c_{i,l}}{t_l})^{-1}}-1\right)\right]^+\\&=\underbrace{\left[-t_l\frac{P_{\max}}{\exp(-\tau P_0+\nu)}\left(\frac{1+\exp(-\tau P_0+\nu)}{1+\exp(\nu)(\frac{c_{i,l}}{t_l})^{-1}}-1\right)\right]^-}_{:=H(c_{i,l},t_l)},\end{aligned} \tag{32}$$

and it is proved in Appendix B that $H(c_{i,l},t_l)$ is convex. So, we only need to focus on the operators $[\cdot]^-$ in (31b) and (32). But since $[x]^-=\min(x,0)\le x$, dropping the operators $[\cdot]^-$ would make the feasible set of P2 smaller and the solution of such a problem would provide an inner bound for the achievable rate region $\mathcal{R}(\mathbf{e},\mathcal{H})$.

After the above procedures, the only nonconvex parts in P2 are $\Phi_m(Q_{1,m},Q_{2,m},t_m):=-t_m\log_2\left(1+\frac{\sigma_r^2t_m}{Q_{1,m}+Q_{2,m}}\right)$ in (31b), $\Upsilon_{i,m}(a_{i,m}):=-\frac{1}{a_{i,m}}$ in (31d), $\Xi_{i,m}(\mathbf{w}_m,Q_{i,m}):=-\frac{|\mathbf{w}_m^H\mathbf{h}_{i,m}|^2}{Q_{i,m}}$ in (31f), and $\Psi_{i,m}(c_{i,m},t_m)=\frac{t_m}{\tau}\ln(\frac{c_{i,m}}{t_m})$ in (31g). Fortunately, we have the following property (proved in Appendix C) for those terms.

Property 3: The functions Φ_m, $\Upsilon_{i,m}$, $\Xi_{i,m}$, *and* $\Psi_{i,m}$ *are concave.*

Since Φ_m, $\Upsilon_{i,m}$, $\Xi_{i,m}$, and $\Psi_{i,m}$ are concave, we can apply the majorization technique [37]–[39] to replace them with convex upper bounds, which further reduce the feasible set of P2. More specifically, given any feasible solution $\{t_m^\star,\mathbf{w}_m^\star,Q_{i,m}^\star,a_{i,m}^\star,c_{i,m}^\star\}$ of P2, we define surrogate functions $\tilde{\Phi}_m,\tilde{\Upsilon}_{i,m},\tilde{\Xi}_{i,m},\tilde{\Psi}_{i,m}$ as

$$\begin{aligned}&\tilde{\Phi}_m(Q_{1,m},Q_{2,m},t_m|Q_{1,m}^\star,Q_{2,m}^\star,t_m^\star)\\&:=-t_m^\star\log_2\left(1+\frac{\sigma_r^2t_m^\star}{Q_{1,m}^\star+Q_{2,m}^\star}\right)\\&\quad+\frac{(t_m^\star)^2/\ln 2}{t_m^\star(Q_{1,m}^\star+Q_{2,m}^\star)+(Q_{1,m}^\star+Q_{2,m}^\star)^2/\sigma_r^2}\\&\quad\times\left(Q_{1,m}+Q_{2,m}-Q_{1,m}^\star-Q_{2,m}^\star\right)\\&\quad+\left[-\log_2\left(1+\frac{\sigma_r^2t_m^\star}{Q_{1,m}^\star+Q_{2,m}^\star}\right)-\frac{\sigma_r^2t_m^\star/\ln 2}{\sigma_r^2t_m^\star+Q_{1,m}^\star+Q_{2,m}^\star}\right]\\&\quad\times\left(t_m-t_m^\star\right),\end{aligned} \tag{33}$$

$$\tilde{\Upsilon}_{i,m}(a_{i,m}|a_{i,m}^\star):=-\frac{2}{a_{i,m}^\star}+\frac{1}{(a_{i,m}^\star)^2}a_{i,m}, \tag{34}$$

$$\begin{aligned}&\tilde{\Xi}_{i,m}(\mathbf{w}_m,Q_{i,m}|\mathbf{w}_m^\star,Q_{i,m}^\star)\\&:=-2\mathrm{Re}\left(\frac{(\mathbf{w}_m^\star)^H\mathbf{h}_{i,m}\mathbf{h}_{i,m}^H\mathbf{w}_m}{Q_{i,m}^\star}\right)+\frac{|(\mathbf{w}_m^\star)^H\mathbf{h}_{i,m}|^2}{(Q_{i,m}^\star)^2}Q_{i,m},\end{aligned} \tag{35}$$

$$\begin{aligned}&\tilde{\Psi}_{i,m}(c_{i,m},t_m|c_{i,m}^\star,t_m^\star)\\&:=\frac{t_m^\star}{\tau}\ln\left(\frac{c_{i,m}^\star}{t_m^\star}\right)+\frac{t_m^\star}{\tau c_m^\star}(c_m-c_m^\star)+\left[\frac{1}{\tau}\ln\left(\frac{c_{i,m}^\star}{t_m^\star}\right)-\frac{1}{\tau}\right](t_m-t_m^\star).\end{aligned} \tag{36}$$

By applying the result of **Property 3** and the first-order condition for concave functions, we immediately have

$$\begin{aligned}\tilde{\Phi}_m(Q_{1,m},Q_{2,m},t_m|Q_{1,m}^\star,Q_{2,m}^\star,t_m^\star)&\ge\Phi_m(Q_{1,m},Q_{2,m},t_m),\\\tilde{\Upsilon}_{i,m}(a_{i,m}|a_{i,m}^\star)&\ge\Upsilon_{i,m}(a_{i,m}),\\\tilde{\Xi}_{i,m}(\mathbf{w}_m,Q_{i,m}|\mathbf{w}_m^\star,Q_{i,m}^\star)&\ge\Xi_{i,m}(\mathbf{w}_m,Q_{i,m}),\\\tilde{\Psi}_{i,m}(c_{i,m},t_m|c_{i,m}^\star,t_m^\star)&\ge\Psi_{i,m}(c_{i,m},t_m).\end{aligned} \tag{37}$$

With the above observation, an inner bound can be directly obtained if we replace the functions $\{\Phi_m,\Upsilon_{i,m},\Xi_{i,m},\Psi_{i,m}\}$ by $\{\tilde{\Phi}_m,\tilde{\Upsilon}_{i,m},\tilde{\Xi}_{i,m},\tilde{\Psi}_{i,m}\}$ expanded around a feasible point. However, a tighter inner bound can be achieved if we treat the obtained solution as another feasible point and continue to construct the next round surrogate functions. In particular,

assuming that the solution at the n^{th} iteration is given by $\{t_m^{[n]}, \mathbf{w}_m^{[n]}, Q_{i,m}^{[n]}, a_{i,m}^{[n]}, c_{i,m}^{[n]}\}$, the following problem is considered at the $(n+1)^{\text{th}}$ iteration

$$\text{P2}[n+1]: \max_{\substack{R_{\text{sum}},\{t_m,\mathbf{V}_m,\mathbf{w}_m,Q_{i,m},\omega_{i,m}\},\\ \{r_{i,m},a_{i,m},b_{i,m},c_{i,m}\}}} R_{\text{sum}}$$

$$\text{s.t. } \mu_i R_{\text{sum}} - \frac{1}{T}\sum_{m=1}^{M} r_{i,m} \le 0, \quad \forall i \tag{38a}$$

$$r_{i,m} - t_m \log_2\left(\frac{Q_{i,m}}{\sigma_r^2 t_m}\right) + \tilde{\Phi}_m(Q_{1,m}, Q_{2,m}, t_m | Q_{1,m}^{[n]}, Q_{2,m}^{[n]}, t_m^{[n]}) \le 0, \quad \forall i, m \tag{38b}$$

$$r_{3-i,m} - t_m \log_2\left(1 + \frac{a_{i,m}}{t_m}\right) \le 0, \quad \forall i, m \tag{38c}$$

$$\frac{\sigma_u^2}{\text{Tr}(\mathbf{g}_{i,m}\mathbf{g}_{i,m}^H \mathbf{V}_m)} + \frac{\sigma_z^2}{\omega_{i,m}} + \tilde{\Upsilon}_{i,m}(a_{i,m} | a_{i,m}^{[n]}) \le 0, \quad \forall i, m \tag{38d}$$

$$\sum_{l=1}^{m}\left[b_{i,l} + H(c_{i,l}, t_l) + (2t_l + s_l)p_c\right] \le E_i, \quad \forall i, m \tag{38e}$$

$$\frac{1}{b_{i,m}} + \widetilde{\Xi}_{i,m}(\mathbf{w}_m, Q_{i,m} | \mathbf{w}_m^{[n]}, Q_{i,m}^{[n]}) \le 0, \quad \forall i, m \tag{38f}$$

$$\text{Tr}(\mathbf{g}_{i,m}\mathbf{g}_{i,m}^H \mathbf{V}_m) - \omega_{i,m} \ge \widetilde{\Psi}_{i,m}(c_{i,m}, t_m | c_{i,m}^{[n]}, t_m^{[n]}), \quad \forall i, m \tag{38g}$$

$$(31\text{h}) - (31\text{j}). \tag{38h}$$

Now, except for the second and third constraints, all the constraints in P2$[n+1]$ are obviously convex. However, it can be seen that $-t_m \log_2\left(\frac{Q_{i,m}}{\sigma_r^2 t_m}\right)$ is the perspective of the convex function $-\log_2\left(\frac{Q_{i,m}}{\sigma_r^2}\right)$ and $-t_m \log_2\left(1 + \frac{a_{i,m}}{t_m}\right)$ is the perspective of the convex function $-\log_2\left(1 + a_{i,m}\right)$. Since the perspective operation preserves convexity [40], problem P2$[n+1]$ is convex and can be solved by CVX MOSEK [40], a Matlab software package for solving convex problems. Denoting its optimal solution as $\{t_m^*, \mathbf{w}_m^*, Q_{i,m}^*, a_{i,m}^*, c_{i,m}^*\}$, then we can set $\{t_m^{[n+1]} = t_m^*, \mathbf{w}_m^{n+1} = \mathbf{w}_m^*, Q_{i,m}^{[n+1]} = Q_{i,m}^*, a_{i,m}^{[n+1]} = a_{i,m}^*, c_{i,m}^{[n+1]} = c_{i,m}^*\}$, and the process repeats with solving the problem P2$[n+2]$. According to [37, Th. 1] and condition (37), this iterative algorithm is guaranteed to converge monotonically.

Finally, for the above algorithm, we need a feasible starting point $\{t_m^{[0]}, \mathbf{w}_m^{[0]}, Q_{i,m}^{[0]}, a_{i,m}^{[0]}, c_{i,m}^{[0]}\}$. By applying the penalty method [38, Sec. 3], a feasible $\{t_m^{[0]}, \mathbf{w}_m^{[0]}, Q_{i,m}^{[0]}, a_{i,m}^{[0]}, c_{i,m}^{[0]}\}$ can be found and the detailed procedure is given in Appendix D. The entire iterative procedure for computing the inner bound when $M \ge 2$ is summarized in Algorithm 2.

In terms of computational effort, solving P2$[n+1]$ is dominated by $\{\mathbf{V}_m\}$, which has M semidefinite cones of dimension N and $2M$ linear terms. Therefore, its dual form has $2M$ variables and one semidefinite constraint consisting of M blocks with sizes $N \times N$ [40]. By applying the result from [41, Sec. 6.63], the complexity for solving P2$[n+1]$ can be computed to be $O\left[(1+MN)^{1/2}(8M^3 + 4M^3N^2 + 2M^2N^3)\right]$. As a consequence, the total complexity for solving P2 is $O\left[p(1+MN)^{1/2}(8M^3 + 4M^3N^2 + 2M^2N^3)\right]$, where p is the number of iterations needed for the majorization method to converge.

Algorithm 2 Computing the Inner Bound for $\mathcal{R}(\mathbf{e}, \mathcal{H})$

1: **Given** $\mathbf{e}$, $\mathcal{H}$ and parameters T, p_c, $\{s_m\}$, E_G, E_c, μ_1.
2: **Initialize** $\{t_m^{[0]}, \mathbf{w}_m^{[0]}, Q_{i,m}^{[0]}, a_{i,m}^{[0]}, c_{i,m}^{[0]}\}$ according to Appendix D and set $n = 0$.
3: **Repeat**
4: Update $\{t_m^{[n+1]}, \mathbf{w}_m^{[n+1]}, Q_{i,m}^{[n+1]}, a_{i,m}^{[n+1]}, c_{i,m}^{[n+1]}\}$ by solving P2$[n+1]$. Set $n = n+1$.
5: **Until** convergence and the converged point is $R_{\text{sum}}^{\diamond}$.
6: A point on the inner bound boundary is $(\mu_1 R_{\text{sum}}^{\diamond}, \mu_2 R_{\text{sum}}^{\diamond})$.
7: **Vary** μ_1 from 0 to 1 and repeat the above steps.

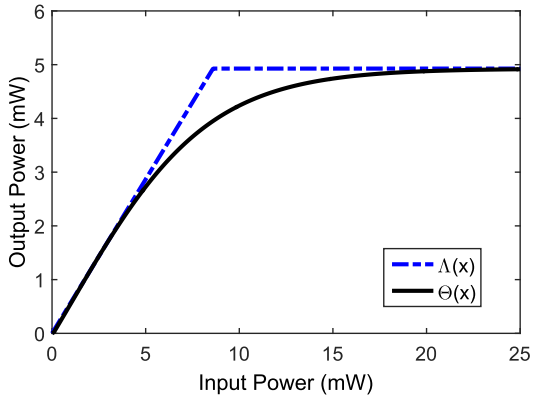

Fig. 4. Illustration of Θ and Λ.

Remark: In this paper, the main focus is the achievable rate region analysis of wirelessly powered TWRC under fixed or mobile relay. Therefore, complexity is not the utmost consideration. However, if N is so large that the semidefinite programming is not possible to be carried out, we can apply the method in [2, Sec. IV-A] to reduce the dimension of $\mathbf{V}_m$ from $N \times N$ to 2×2.

B. Outer Bound

Besides the proposed inner bound of the achievable rate region, we also need an outer bound to locate the achievable rate region $\mathcal{R}(\mathbf{e}, \mathcal{H})$. To achieve this goal, the major challenge is the nonlinear function Θ in (31e) of P2, and we propose to use a piecewise linear function $\Lambda(x) = \min(\zeta x, P_{\max})$ to bound Θ from above as shown in Fig. 4. In order to choose ζ such that Λ is as tight as possible, the following problem is considered:

$$\min_{\zeta \ge 0} \ \zeta \quad \text{s.t. } \min(\zeta x, P_{\max}) \ge \Theta(x), \quad \forall x \ge 0. \tag{39}$$

Since the above problem only has one scalar variable ζ, a bisection search algorithm similar to that of Section IV-A can be applied, and the optimal solution is denoted as ζ^*.

With the function Θ replaced by Λ, we will further apply four relaxations to enlarge the feasible set of P2, and such

relaxations would provide an outer bound for $\mathcal{R}(\mathbf{e}, \mathcal{H})$:

(i) Using $\frac{\sigma_r^2 t_m}{Q_{1,m}+Q_{2,m}} \leq \frac{\sigma_r^2 t_m}{Q_{i,m}}$, the constraint (31b) can be relaxed to $r_{i,m} + [-t_m \log_2(1+\frac{Q_{i,m}}{\sigma_r^2 t_m})]^- \leq 0$. Furthermore, due to $\log_2(1+\frac{Q_{i,m}}{\sigma_r^2 t_m}) \geq 0$, the operator $[\cdot]^-$ can be dropped without changing the constraint;

(ii) Using $\mathrm{Tr}(\mathbf{g}_{i,m}\mathbf{g}_{i,m}^H \mathbf{V}_m) \geq \omega_{i,m}$ due to (31g), (31d) is relaxed into $\frac{\sigma_u^2+\sigma_z^2}{\mathrm{Tr}(\mathbf{g}_{i,m}\mathbf{g}_{i,m}^H \mathbf{V}_m)} \leq \frac{1}{a_{i,m}}$;

(iii) Applying $|\mathbf{w}_m^H \mathbf{h}_{i,m}|^2 \leq ||\mathbf{h}_{i,m}||^2$ (due to $||\mathbf{w}_m|| = 1$) to (31f), the relaxed constraint becomes $Q_{i,m} \leq b_{i,m}||\mathbf{h}_{i,m}||^2$.

(iv) Since $\omega_{i,m} \geq 0$, the constraint $\mathrm{Tr}(\mathbf{g}_{i,m}\mathbf{g}_{i,m}^H \mathbf{V}_m) - \omega_{i,m} \geq \frac{t_m}{\tau}\ln(\frac{c_{i,m}}{t_m})$ in (31g) can be relaxed into $\mathrm{Tr}(\mathbf{g}_{i,m}\mathbf{g}_{i,m}^H \mathbf{V}_m)/t_m \geq \frac{1}{\tau}\ln(\frac{c_{i,m}}{t_m})$. Combining this constraint and (31e) into one constraint, we obtain $\sum_{l=1}^m \left\{ b_{i,l} - t_l \Lambda\left(\mathrm{Tr}(\mathbf{g}_{i,m}\mathbf{g}_{i,m}^H \mathbf{V}_m)/t_m\right) + (2t_l + s_l)p_c \right\} \leq E_i$.

After the above relaxations, the following outer bound problem of P2 is obtained:

$$\mathrm{P3}: \max_{R_{\mathrm{sum}}, \{t_m, \mathbf{V}_m, Q_{i,m}\}, \{r_{i,m}\}} R_{\mathrm{sum}}$$

$$\text{s.t. } \mu_i R_{\mathrm{sum}} - \frac{1}{T}\sum_{m=1}^M r_{i,m} \leq 0, \quad \forall i \tag{40a}$$

$$r_{i,m} - t_m \log_2\left(1+\frac{Q_{i,m}}{\sigma_r^2 t_m}\right) \leq 0, \quad \forall i, m \tag{40b}$$

$$r_{3-i,m} - t_m \log_2\left(1+\frac{\mathrm{Tr}(\mathbf{g}_{i,m}\mathbf{g}_{i,m}^H \mathbf{V}_m)}{(\sigma_u^2+\sigma_z^2)t_m}\right) \leq 0, \forall i, m \tag{40c}$$

$$\sum_{l=1}^m \left(\frac{Q_{i,l}}{||\mathbf{h}_{i,l}||^2} + \max[-\zeta^* \mathrm{Tr}(\mathbf{g}_{i,l}\mathbf{g}_{i,l}^H \mathbf{V}_l), -t_l P_{\max}] + (2t_l + s_l)p_c \right) \leq E_i, \quad \forall i, m \tag{40d}$$

$$E_G + E_c + \sum_{m=1}^M \mathrm{Tr}(\mathbf{V}_m) \leq E_r, \sum_{m=1}^M (2t_m + s_m) = T \tag{40e}$$

$$\mathbf{V}_m \succeq 0, \ t_m \geq 0, \quad \forall m, \ Q_{i,m} \geq 0, \ \forall i, m. \tag{40f}$$

Because P3 only contains linear, semidefinite, relative entropy, and maximum functions, problem P3 is convex and can be solved by the existing software. Interestingly, it can be seen from the constraints (40b) and (40c) that P3 also provides an outer bound for the amplify-and-forward scheme and the decode-and-forward scheme. The procedure to compute the outer bound is summarized in Algorithm 3.

Algorithm 3 Computing the Outer Bound for $\mathcal{R}(\mathbf{e}, \mathcal{H})$

1: **Given** $\mathbf{e}$, $\mathcal{H}$ and parameters T, p_c, $\{s_m\}$, E_G, E_c, μ_1.
2: Solve P3 and the optimal value is given by R'_{sum}. A point on the boundary of outer bound is obtained as $(\mu_1 R'_{\mathrm{sum}}, \mu_2 R'_{\mathrm{sum}})$.
3: **Vary** μ_1 from 0 to 1 and repeat the above steps.

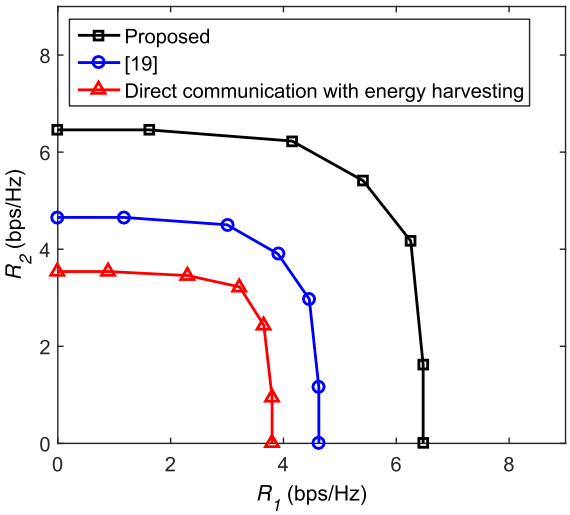

Fig. 5. Achievable rate region for wirelessly powered TWRC with a fixed relay.

VI. Numerical Results and Discussions

This section provides numerical results to illustrate the derived achievable rate regions. In particular, the distance-dependent path-loss model of user i $\varrho_{i,m} = \varrho_0 \cdot (\frac{d_{i,m}}{d_0})^{-\alpha}$ is adopted, where $d_{i,m}$ is the distance from user i to the m^{th} stopping point of the relay, $\varrho_0 = 10^{-3}$, $d_0 = 1$ m is the reference distance, and α is the path-loss exponent set to be 2.7 [2], [4]. Based on the path-loss model, channels $\mathbf{g}_{i,m}$ and $\mathbf{h}_{i,m}$ are generated according to $\mathcal{CN}(\mathbf{0}, \varrho_{i,m}\mathbf{I}_N)$. The parameters in the energy harvesting model are obtained by fitting the experimental data from the Powercast energy harvester P2110 [28] to the model, and they are given by $\tau = 274$, $\nu = 0.29$, $P_{\max} = 0.004927$ W and $P_0 = 0.000064$ W. By using these parameters, we can further compute $\zeta^* = 0.5732$. It is assumed that the circuit power $p_c = 10$ dBm and the relay circuit energy $E_c = 100$ J. The receiver noise powers are set to $\sigma_r^2 = \sigma_u^2 = -70$ dBm (corresponding to power spectral density -140 dBm/Hz with 10 MHz bandwidth), which include thermal noise, intermodulation noise, crosstalk and impulse noise [42, p. 109]. The thermal noise at the power splitter is set to $\sigma_z^2 = -104$ dBm (corresponding to power spectral density -174 dBm/Hz with 10 MHz bandwidth). Furthermore, within the duration $T = 50$ s, the energy available at the relay is $E_r = 300$ J while the energies available at users are $E_i \sim \mathcal{U}(400, 800)$ in mJ, where $\mathcal{U}$ represents the uniform distribution. Each point in the figures is obtained by averaging over 100 simulation runs, with independent channels and realizations of E_i in each run.

First, we consider the fixed relay case $M = 1$ with $N = 8$. Specifically, the distance between the two users is 5 meters and the relay is randomly located between the two users. The new achievable rate region computed via Algorithm 1 is compared to the achievable rate region without energy harvesting [19] and the achievable rate region using direct communication

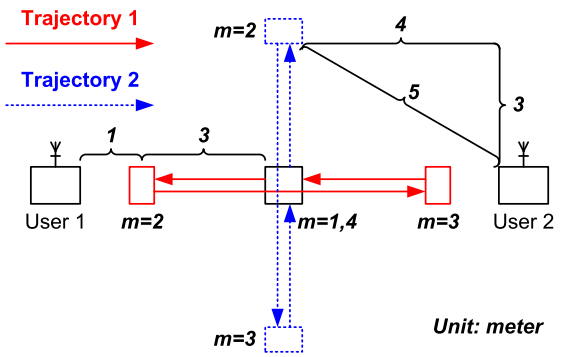

Fig. 6. Two moving trajectories of relay with $M = 4$.

with energy harvesting.[4] It is observed from Fig. 5 that the newly established achievable rate region encloses the rate region of [19]. The performance improvement demonstrates the advantage of employing WPT at the TWRC, while the performance gap concisely quantifies the achievable rate gain brought by energy harvesting. On the other hand, the direct communication performs poorly because the transmit powers at users are much lower than that of the relay, which leads to small data-rates of direct links. To mitigate this problem, the users may first offload the data to the relay and then the relay forwards the data to the destination.

Next, we consider the moving relay case $M \geq 2$ and $N = 8$ with the setting shown in Fig. 6. The distance between the two users is 8 meters, while the initial position of the relay is 4 meters away from both users. We consider two trajectories. Starting from the initial position, the relay either moves along a horizontal or vertical trajectory, with each trajectory having $M = 4$ stopping points marked with squares. Since the length of different sections are $(3, 6, 3)$ m, the moving time would be $(s_1, s_2, s_3) = (1.5, 3, 1.5)$ s with a relay velocity of $v = 2$ m/s [22]. Furthermore, based on the power model for Pioneer 3DX robot [23, Sec. IV-C], the motion power can be computed to be $0.29 + 7.4v = 15.09$ W, and the required motion energy is therefore $E_G = 15.09 \times 6 = 90.54$ J.

Under the trajectories defined above, the convergence of the Algorithm 2 in Section V is shown in Fig. 7 when $\mu_1 = \mu_2 = 0.5$. It can be seen that the iterative Algorithm 2 converges after 20 iterations. Therefore, the number of iterations is set to be 20 for the rest of this section.

On the other hand, the achievable rate region of fixed relay using Algorithm 1 and the rate region bounds of mobile relay using Algorithms 2 and 3 are compared in Fig. 8. It can be seen that the inner bound of the moving relay case is very close to the corresponding outer bound no matter which trajectory the relay takes. Furthermore, of the two trajectories, the rate region of trajectory 1 outperforms the achievable rate of fixed relay significantly. This shows the potential advantage of enabling mobility in wirelessly powered TWRC. However, when the relay is moving along the second trajectory, both the inner bound and outer bound of the rate region are smaller than the

[4]For this scheme, the users communicate directly and may also be charged via the relay.

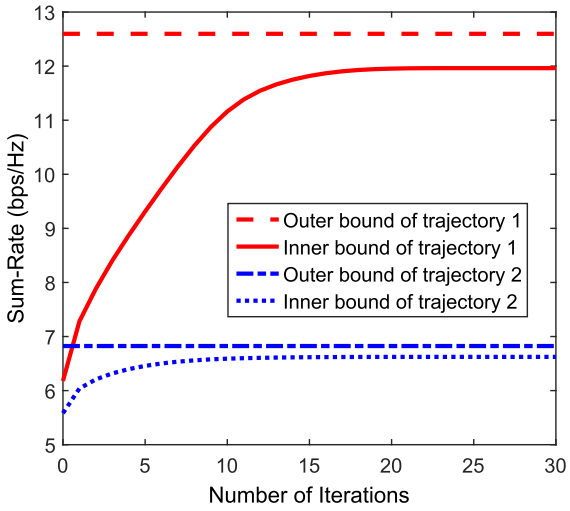

Fig. 7. Sum-rate versus number of iterations for computing the inner bound using Algorithm 2.

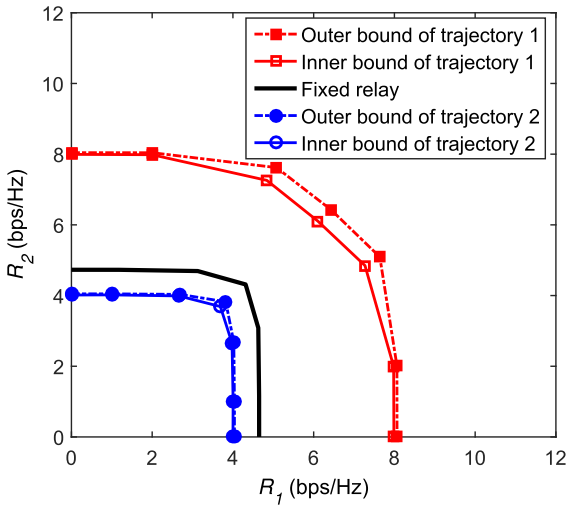

Fig. 8. Rate bounds for wirelessly powered TWRC with a moving relay, and exact achievable rate region of wirelessly powered TWRC with a fixed relay.

achievable rate region of the fixed relay. This indicates that moving is not always beneficial. In fact, it highly depends on the trajectory and the required motion energy relative to the available energy at relay.

In order to illustrate the last point, the sum-rate versus the available relay energy with $\mu_1 = \mu_2 = 0.5$ is shown in Fig. 9. It can be observed that when the relay energy is small, even moving along trajectory 1 deteriorates the performance compared to the fixed relay case since the additional motion energy consumption depletes the energy for transmission. However, when the available relay energy exceeds the sum of circuit energy and motion energy, a slight increase of relay energy would enable the sum-rate to exceed that of the fixed relay, which increases much slower as shown in Fig. 9. This result implies that there exists a trade-off between spending energy on moving and on transmission.

To get more insights into the trade-off, it is proved in Appendix E that a closed-form upper bound for R_{sum}

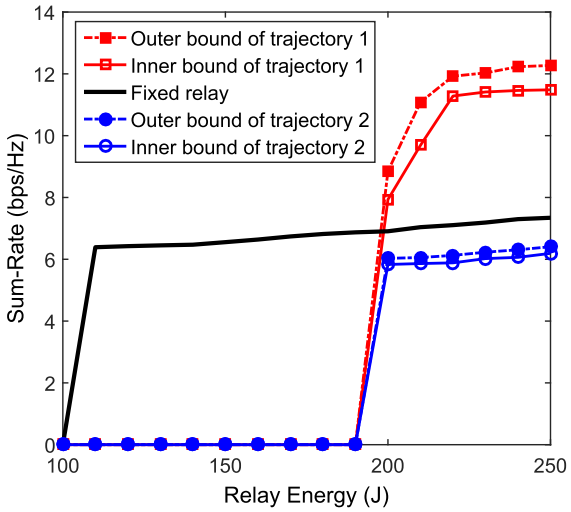

Fig. 9. Sum-rate versus available relay energy for fixed relay and mobile relay.

in P1 is

$$R_{\text{sum}} \le \min_{i=1,2} \frac{1}{2\mu_i} \min \left[\log_2\left(1+\frac{2h_i^{\max}[E_i - T p_c + \zeta^* g_i^{\max}(E_r - E_G - E_c)]}{\sigma_r^2 T}\right), \log_2\left(1+\frac{2g_{3-i}^{\max}(E_r - E_G - E_c)}{(\sigma_u^2+\sigma_z^2)T}\right)\right], \quad (41)$$

where $h_i^{\max} = \max_{m=1,\ldots,M} ||\mathbf{h}_{i,m}||^2$ and $g_i^{\max} = \max_{m=1,\ldots,M} ||\mathbf{g}_{i,m}||^2$. From (41), it is observed that if moving (i.e., increasing E_G) does not lead to improved channels (in terms of $h_i^{\max}$ and $g_i^{\max}$), the bound would decrease, thus moving in this way might not be beneficial. This corroborates with the result of trajectory 2, in which $h_i^{\max}$ and $g_i^{\max}$ do not change but E_G increases from 0 to 90.54J. On the other hand, if moving leads to improved channels such that there is a net increase in $g_i^{\max}(E_r - E_G - E_c)$ for both $i = 1, 2$, the bound would increase, and the system might be benefited from the moving relay. This is the case for trajectory 1. While the above discussion provides a rough guideline to determine which trajectory is a good one, Algorithms 1-3 allow us to precisely figure out how much gain can be obtained from mobile relay along a particular trajectory.

VII. Conclusions

This paper studied the achievable rate region of wirelessly powered TWRC. For the case of fixed relay, the exact achievable rate region was obtained using bisection algorithm, with closed-form solutions in each iteration. For the case of moving relay, given a moving trajectory, a pair of inner and outer rate bounds were derived, and the rate bounds can be used to locate the achievable rate region. Numerical results showed that the new achievable rate region of wirelessly powered TWRC encloses the existing achievable rate region without energy harvesting. Moreover, with appropriate trajectory, the relay movement can further enlarge the achievable rate region of TWRC.

Appendix A
Proof of Property 2

To prove the property, we only need to focus on the constraints of P2 that are related to $\mathbf{V}_m$, which are given by (31d), (31g), and (31h). In particular, the constraint (31d) can be rearranged as $\text{Tr}(\mathbf{g}_{i,m}\mathbf{g}_{i,m}^H \mathbf{V}_m) \ge \sigma_u^2 (\frac{1}{a_{i,m}} - \frac{\sigma_z^2}{\omega_{i,m}})^{-1}$ and the constraint (31g) can be rewritten as $\text{Tr}(\mathbf{g}_{i,m}\mathbf{g}_{i,m}^H \mathbf{V}_m) \ge t_m \ln(\frac{c_{i,m}}{t_m}) + \omega_{i,m}$. Now, consider the following semidefinite programming problem

$$\begin{aligned} &\text{find } \{\mathbf{V}_m \succeq 0\} \\ &\text{s.t. } \text{Tr}(\mathbf{g}_{i,m}\mathbf{g}_{i,m}^H \mathbf{V}_m) \ge \max\left[\sigma_u^2\left(\frac{1}{a_{i,m}^*} - \frac{\sigma_z^2}{\omega_{i,m}^*}\right)^{-1}, \right. \\ &\left. t_m^* \ln\left(\frac{c_{i,m}^*}{t_m^*}\right) + \omega_{i,m}^*\right], \quad \forall i, m \\ &E_G + E_c + \sum_{m=1}^{M} \text{Tr}(\mathbf{V}_m) \le E_r, \end{aligned} \quad (42)$$

where $\{t_m^*, \omega_{i,m}^*, a_{i,m}^*, c_{i,m}^*\}$ are the optimal solution to the rank relaxed problem of P2, and the constraints of (42) are obtained by taking intersection of (31d), (31g), and (31h).

Since problem (42) is equivalent to the rank relaxed problem of P2 with $\{t_m = t_m^*, \omega_{i,m} = \omega_{i,m}^*, a_{i,m} = a_{i,m}^*, c_{i,m} = c_{i,m}^*\}$, problem (42) and the rank relaxed problem of P2 must have the same optimal solution $\{\mathbf{V}_m^*\}$. On the other hand, problem (42) has all together three constraints on each $\mathbf{V}_m$. According to [36, Th. 3.2], there exists $\mathbf{V}_m^*$ with $\text{Rank}^2(\mathbf{V}_m^*) \le 3$, which yields $\text{Rank}(\mathbf{V}_m^*) \le \sqrt{3}$, and $\text{Rank}(\mathbf{V}_m^*) \le 1$ holds.

Appendix B
Proof of Convexity for $H(x, t)$

Based on the definition of H in (32), $H(x, t)$ is the perspective transformation of $I(x)$ in terms of t, where

$$I(x) = -\frac{P_{\max}}{\exp(-\tau P_0 + \nu)}\left(\frac{1+\exp(-\tau P_0+\nu)}{1+\exp(\nu)x^{-1}} - 1\right). \quad (43)$$

Therefore, $H(x, t)$ and $I(x)$ have the save convex property [40], and we only need to focus on $I(x)$. In particular, $I(x)$ can be reformulated as

$$I(x) = \frac{P_{\max}}{\exp(-\tau P_0+\nu)} - \frac{P_{\max}[1+\exp(-\tau P_0+\nu)]}{\exp(-\tau P_0+\nu)} + \frac{P_{\max}[1+\exp(-\tau P_0+\nu)]}{\exp(-\tau P_0+\nu)} \cdot \frac{\exp(\nu)}{x+\exp(\nu)}. \quad (44)$$

Since the term $\frac{\exp(\nu)}{x+\exp(\nu)}$ is convex in x for $x \ge 0$, $I(x)$ is a convex function. As a consequence, $H(x, t)$ is convex.

Appendix C
Proof of Property 3

To prove the property, we first show that Φ_m is concave. More specifically, since Φ_m is the perspective of $-\log_2\left(1 + \frac{\sigma_r^2}{Q_{1,m}+Q_{2,m}}\right)$, which is the composition with an affine mapping $x = Q_{1,m} + Q_{2,m}$ from the function $f(x) =$

$-\log_2\left(1+\frac{\sigma_r^2}{x}\right)$ with $x>0$, Φ_m has the same convex property as $f(x)$. Furthermore, due to $\nabla^2 f(x)=-\frac{\sigma_r^2}{\ln 2}(x^2+\sigma_r^2 x)^{-2}(2x+\sigma_r^2)<0$, $f(x)$ is a concave function. As a result, Φ_m is a concave function with respect to $Q_{1,m}, Q_{2,m}, t_m$.

Secondly, we will show that $\Upsilon_{i,m}$ is concave. By taking the second order derivative of $\Upsilon_{i,m}$ with respect to $a_{i,m}$, we have $\nabla^2\Upsilon_{i,m}=-2a_{i,m}^{-3}$. Since $a_{i,m}$ defined above P2 satisfies $\frac{1}{a_{i,m}}\geq\frac{\sigma_u^2}{\mathrm{Tr}(\mathbf{g}_{i,m}\mathbf{g}_{i,m}^H\mathbf{V}_m)}+\frac{\sigma_z^2}{\omega_{i,m}}$, we have $a_{i,m}\geq 0$ (due to $\mathrm{Tr}(\mathbf{g}_{i,m}\mathbf{g}_{i,m}^H\mathbf{V}_m)\geq 0$ and $\omega_{i,m}\geq 0$). Therefore, $\nabla^2\Upsilon_{i,m}\leq 0$ and $\Upsilon_{i,m}$ is concave.

Thirdly, we will show that $\Xi_{i,m}$ is concave. In particular, since the term $-\Xi_{i,m}=\frac{|\mathbf{w}_m^H\mathbf{h}_{i,m}|^2}{Q_{i,m}}$ is the perspective of a convex quadratic function $|\mathbf{w}_m^H\mathbf{h}_{i,m}|^2$ [40, Ch. 3.2.6], $-\Xi_{i,m}$ is convex. Using the fact that a concave function is the negative of a convex function [40, Ch. 3], $\Xi_{i,m}$ is concave.

Finally, $\Psi_{i,m}$ is concave because the term $\Psi_{i,m}(c_{i,m},t_m)=\frac{t_m}{\tau}\ln(\frac{c_{i,m}}{t_m})$ is the perspective of a concave function $\frac{1}{\tau}\ln(c_{i,m})$. This completes the proof.

Appendix D
Initialization for Algorithm 2

The penalty method adopts an iterative procedure to find a feasible point for the majorization algorithm. In particular, at the n^{th} iteration, the penalty method solves the following problem:

$$\begin{aligned}\max_{\substack{R_{\mathrm{sum}},\{t_m,\mathbf{V}_m,\mathbf{w}_m,Q_{i,m},\omega_{i,m}\},\\ \{r_{i,m},a_{i,m},b_{i,m},c_{i,m}\},\{\varphi_{i,m}\}}} & R_{\mathrm{sum}}-\epsilon\sum_{i=1}^{2}\sum_{m=1}^{M}\varphi_{i,m}\\ \text{s.t. } & (38a)-(38d),\ (38f)-(38h)\\ & \sum_{l=1}^{m}\Big[b_{i,l}+H(c_{i,l},t_l)+(2t_l+s_l)p_c\Big]\\ & \leq E_i+\varphi_{i,m},\quad \forall i,m,\end{aligned}$$

where the penalty ϵ is sufficiently large (e.g., $\epsilon=10^6$). The above iterative procedure is started by any $\{t_m',\mathbf{w}_m',Q_{i,m}',a_{i,m}',c_{i,m}'\}$ satisfying (31h)-(31j), and is terminated until $\sum_{i=1}^{2}\sum_{m=1}^{M}\varphi_{i,m}$ is sufficiently small, e.g., less than 10^{-10}. The last round solution is then used as the initial point $\{t_m^{[0]},\mathbf{w}_m^{[0]},Q_{i,m}^{[0]},a_{i,m}^{[0]},c_{i,m}^{[0]}\}$ for P2[1].

Appendix E
Proof of Equation (41)

We prove (41) by applying a series of relaxations to the constraints of P1. First, using $\frac{q_{i,m}|\mathbf{w}_m^H\mathbf{h}_{i,m}|^2}{\sum_{j=1}^{2}q_{j,m}|\mathbf{w}_m^H\mathbf{h}_{j,m}|^2}\leq 1$, $\frac{\beta_{3-i,m}p_m|\mathbf{g}_{3-i,m}^H\mathbf{v}_m|^2}{\sigma_u^2\beta_{3-i,m}+\sigma_z^2}\leq\frac{p_m||\mathbf{g}_{3-i,m}||^2}{\sigma_u^2+\sigma_z^2}$ (due to $\beta_{3-i,m}\leq 1$ and $||\mathbf{v}_m||=1$), and $|\mathbf{w}_m^H\mathbf{h}_{i,m}|^2\leq||\mathbf{h}_{i,m}||^2$ (due to $||\mathbf{w}_m||=1$), the first constraint of P1 is relaxed into

$$\frac{1}{T}\sum_{m=1}^{M}\min\left\{t_m\log_2\left(1+\frac{q_{i,m}||\mathbf{h}_{i,m}||^2}{\sigma_r^2}\right),\ t_m\log_2\left(1+\frac{p_m||\mathbf{g}_{3-i,m}||^2}{\sigma_u^2+\sigma_z^2}\right)\right\}\geq\mu_i R_{\mathrm{sum}}.$$

Now, exchanging the operators $\sum_{m=1}^{M}$ and min, and by applying Jensen's Inequality, the above inequality is further relaxed into

$$\frac{\sum_{m=1}^{M}t_m}{T}\min\left\{\log_2\left(1+\frac{\sum_{m=1}^{M}t_m q_{i,m}||\mathbf{h}_{i,m}||^2}{\sigma_r^2\sum_{m=1}^{M}t_m}\right),\ t_m\log_2\left(1+\frac{\sum_{m=1}^{M}t_m p_m||\mathbf{g}_{3-i,m}||^2}{(\sigma_u^2+\sigma_z^2)\sum_{m=1}^{M}t_m}\right)\right\}\geq\mu_i R_{\mathrm{sum}}.\quad(45)$$

On the other hand, from the second constraint of P1 and using $\Lambda(x)\geq\Theta(x)$ for all $x\geq 0$, we have $\sum_{m=1}^{M}t_m q_{i,m}||\mathbf{h}_{i,m}||^2\leq h_i^{\max}(E_i-Tp_c+\zeta^*\sum_{m=1}^{M}t_m p_m||\mathbf{g}_{i,m}||^2)$, and from the third constraint of P1, we have $\sum_{m=1}^{M}t_m p_m||\mathbf{g}_{i,m}||^2\leq g_i^{\max}(E_r-E_G-E_c)$. Putting the above results and $\sum_{m=1}^{M}2t_m\leq T$ into (45), we immediately obtain (41).

References

[1] V. Jamali, N. Zlatanov, and R. Schober, "Bidirectional buffer-aided relay networks with fixed rate transmission—Part I: Delay-unconstrained case," *IEEE Trans. Wireless Commun.*, vol. 14, no. 3, pp. 1323–1338, Mar. 2015.

[2] S. Wang, M. Xia, and Y.-C. Wu, "Multi-pair two-way relay network with harvest-then-transmit users: Resolving pairwise uplink-downlink coupling," *IEEE J. Sel. Topics Signal Process.*, vol. 10, no. 8, pp. 1506–1521, Dec. 2016.

[3] X. Lu, P. Wang, D. Niyato, D. I. Kim, and Z. Han, "Wireless networks with RF energy harvesting: A contemporary survey," *IEEE Commun. Surveys Tuts.*, vol. 17, no. 2, pp. 757–789, 2nd Quart., 2015.

[4] D. W. K. Ng and R. Schober, "Secure and green SWIPT in distributed antenna networks with limited backhaul capacity," *IEEE Trans. Wireless Commun.*, vol. 14, no. 9, pp. 5082–5097, Sep. 2015.

[5] M. Xia and S. Aïssa, "On the efficiency of far-field wireless power transfer," *IEEE Trans. Signal Process.*, vol. 63, no. 11, pp. 2835–2847, Jun. 2015.

[6] S. Bi, C. K. Ho, and R. Zhang, "Wireless powered communication: Opportunities and challenges," *IEEE Commun. Mag.*, vol. 53, no. 4, pp. 117–125, Apr. 2015.

[7] G. Zheng, I. Krikidis, C. Masouros, S. Timotheou, D.-A. Toumpakaris, and Z. Ding, "Rethinking the role of interference in wireless networks," *IEEE Commun. Mag.*, vol. 52, no. 11, pp. 152–158, Nov. 2014.

[8] K. Huang and E. Larsson, "Simultaneous information and power transfer for broadband wireless systems," *IEEE Trans. Signal Process.*, vol. 61, no. 23, pp. 5972–5986, Dec. 2013.

[9] Q. Wu, M. Tao, D. W. K. Ng, W. Chen, and R. Schober, "Energy-efficient resource allocation for wireless powered communication networks," *IEEE Trans. Wireless Commun.*, vol. 15, no. 3, pp. 2312–2327, Mar. 2016.

[10] Q. Wu, W. Chen, D. W. K. Ng, J. Li, and R. Schober, "User-centric energy efficiency maximization for wireless powered communications," *IEEE Trans. Wireless Commun.*, vol. 15, no. 10, pp. 6898–6912, Oct. 2016.

[11] E. Chen, M. Xia, D. B. da Costa, and S. Aïssa, "Multi-hop cooperative relaying with energy harvesting from co-channel interferences," *IEEE Commun. Lett.*, vol. 21, no. 5, pp. 1199–1202, May 2017.

[12] N. Zlatanov, D. W. K. Ng, and R. Schober, "Capacity of the two-hop relay channel with wireless energy transfer from relay to source and energy transmission cost," *IEEE Trans. Wireless Commun.*, vol. 16, no. 1, pp. 647–662, Jan. 2016.

[13] N. Patwari, J. N. Ash, S. Kyperountas, A. O. Hero, R. L. Moses, and N. S. Correal, "Locating the nodes: Cooperative localization in wireless sensor networks," *IEEE Signal Process. Mag.*, vol. 22, no. 4, pp. 54–69, Jul. 2005.

[14] S. Rajasegarar, C. Leckie, and M. Palaniswami, "Anomaly detection in wireless sensor networks," *IEEE Wireless Commun.*, vol. 15, no. 4, pp. 34–40, Aug. 2008.

[15] T. M. Cover and J. A. Thomas, *Elements of Information Theory*. New York, NY, USA: Wiley, 1991.

[16] B. Rankov and A. Wittneben, "Achievable rate regions for the two-way relay channel," in *Proc. IEEE Int. Symp. Inf. Theory*, Seattle, WA, USA, Jul. 2006, pp. 1668–1672.

[17] R. Zhang, Y. C. Liang, C. C. Chai, and S. Cui, "Optimal beamforming for two-way multi-antenna relay channel with analogue network coding," *IEEE J. Sel. Areas Commun.*, vol. 27, no. 5, pp. 699–712, Jun. 2009.
[18] G. Zheng, "Joint beamforming optimization and power control for full-duplex MIMO two-way relay channel," *IEEE Trans. Signal Process.*, vol. 63, no. 3, pp. 555–566, Feb. 2014.
[19] W. Nam, S.-Y. Chung, and Y. H. Lee, "Capacity of the Gaussian two-way relay channel to within 1/2 bit," *IEEE Trans. Inf. Theory*, vol. 56, no. 11, pp. 5488–5494, Nov. 2010.
[20] H. J. Yang, J. Chun, and A. Paulraj, "Asymptotic capacity of the separated MIMO two-way relay channel," *IEEE Trans. Inf. Theory*, vol. 57, no. 11, pp. 7542–7554, Nov. 2011.
[21] Y. Zeng, R. Zhang, and T. J. Lim, "Wireless communications with unmanned aerial vehicles: Opportunities and challenges," *IEEE Commun. Mag.*, vol. 54, no. 5, pp. 36–42, May 2016.
[22] G. Wang, M. J. Irwin, P. Berman, H. Fu, and T. La Porta, "Optimizing sensor movement planning for energy efficiency," in *Proc. Int. Symp. Low Power Electron. Design (ISLPED)*, 2005, pp. 215–220.
[23] Y. Mei, Y.-H. Lu, Y. C. Hu, and C. S. G. Lee, "Deployment of mobile robots with energy and timing constraints," *IEEE Trans. Robot.*, vol. 22, no. 3, pp. 507–522, Jun. 2006.
[24] F. El-Moukaddem, E. Torng, and G. Xing, "Mobile relay configuration in data-intensive wireless sensor networks," *IEEE Trans. Mobile Comput.*, vol. 12, no. 12, pp. 261–273, Feb. 2013.
[25] Y. Yan and Y. Mostofi, "Co-optimization of communication and motion planning of a robotic operation under resource constraints and in fading environments," *IEEE Trans. Wireless Commun.*, vol. 12, no. 4, pp. 1562–1572, Apr. 2013.
[26] A. Bletsas, A. G. Dimitriou, and J. N. Sahalos, "Improving backscatter radio tag efficiency," *IEEE Trans. Microw. Theory Techn.*, vol. 58, no. 6, pp. 1502–1509, Jun. 2010.
[27] J. A. Hagerty, F. B. Helmbrecht, W. H. McCalpin, R. Zane, and Z. B. Popovic, "Recycling ambient microwave energy with broad-band rectenna arrays," *IEEE Trans. Microw. Theory Techn.*, vol. 52, no. 3, pp. 1014–1024, Mar. 2004.
[28] *Powercast Wireless Power Calculator (Version 1.5)*. Accessed: Nov. 2016. [Online]. Available: http://www.powercastco.com/power-calculator/
[29] C. R. Valenta and G. D. Durgin, "Harvesting wireless power: Survey of energy-harvester conversion efficiency in far-field, wireless power transfer systems," *IEEE Microw. Mag.*, vol. 15, no. 4, pp. 108–120, Jun. 2014.
[30] S. D. Assimonis, S. N. Daskalakis, and A. Bletsas, "Sensitive and efficient RF harvesting supply for batteryless backscatter sensor networks," *IEEE Trans. Microw. Theory Techn.*, vol. 64, no. 4, pp. 1327–1338, Apr. 2016.
[31] E. Boshkovska, D. W. K. Ng, N. Zlatanov, and R. Schober, "Practical non-linear energy harvesting model and resource allocation for SWIPT systems," *IEEE Commun. Lett.*, vol. 19, no. 12, pp. 2082–2085, Dec. 2015.
[32] V. Jamali, N. Zlatanov, A. Ikhlef, and R. Schober, "Achievable rate region of the bidirectional buffer-aided relay channel with block fading," *IEEE Trans. Inf. Theory*, vol. 60, no. 11, pp. 7090–7111, Nov. 2014.
[33] K. Xiong, P. Fan, Z. Xu, H.-C. Yang, and K. B. Letaief, "Optimal cooperative beamforming design for MIMO decode-and-forward relay channels," *IEEE Trans. Signal Process.*, vol. 62, no. 6, pp. 1476–1489, Mar. 2014.
[34] K. Xiong, P. Fan, C. Zhang, and K. B. Letaief, "Wireless information and energy transfer for two-hop non-regenerative MIMO-OFDM relay networks," *IEEE J. Sel. Areas Commun.*, vol. 33, no. 8, pp. 1595–1611, Aug. 2015.
[35] Z.-Q. Luo, W.-K. Ma, A. M.-C. So, Y. Ye, and S. Zhang, "Semidefinite relaxation of quadratic optimization problems," *IEEE Signal Process. Mag.*, vol. 27, no. 3, pp. 20–34, May 2010.
[36] Y. Huang and D. P. Palomar, "Rank-constrained separable semidefinite programming with applications to optimal beamforming," *IEEE Trans. Signal Process.*, vol. 58, no. 2, pp. 664–678, Feb. 2010.
[37] B.-R. Marks and G.-P. Wright, "A general inner approximation algorithm for nonconvex mathematical programs," *Oper. Res.*, vol. 26, no. 4, pp. 681–683, Jul. 1978.
[38] T. Lipp and S. Boyd, "Variations and extension of the convex–concave procedure," *Optim. Eng.*, vol. 17, no. 2, pp. 263–287, Jun. 2016.
[39] Y. Sun, P. Babu, and D. P. Palomar, "Majorization-minimization algorithms in signal processing, communications, and machine learning," *IEEE Trans. Signal Process.*, vol. 65, no. 3, pp. 794–816, Feb. 2017, doi: 10.1109/TSP.2016.2601299.
[40] S. Boyd and L. Vandenberghe, *Convex Optimization*. Cambridge, U.K.: Cambridge Univ. Press, 2004.
[41] A. Ben-Tal and A. Nemirovski, *Lectures on Modern Convex Optimization: Analysis, Algorithms, and Engineering Applications* (MPS/SIAM Series on Optimizations). Philadelphia, PA, USA: SIAM, 2013.
[42] W. Stallings, *Wireless Communications and Networks*. Englewood Cliffs, NJ, USA: Prentice-Hall, 2004.

Shuai Wang (S'16) received the B.S. and M.S. degrees in electronic engineering from the Beijing University of Posts and Telecommunications in 2011 and 2014, respectively. He is currently pursuing the Ph.D. degree in electrical and electronic engineering with The University of Hong Kong. His research interests include the signal processing and analysis of wireless networks using optimization.

Minghua Xia (M'12) received the Ph.D. degree in telecommunications and information systems from Sun Yat-sen University, Guangzhou, China, in 2007.

From 2007 to 2009, he was with the Electronics and Telecommunications Research Institute, South Korea, and also with the Beijing Research and Development Center, Beijing, China, where he was a Member and then a Senior Member of Engineering Staff and participated in projects on the physical layer design of 3GPP LTE mobile communications. From 2010 to 2014, he was a Post-Doctoral Fellow with The University of Hong Kong, Hong Kong; the King Abdullah University of Science and Technology, Jeddah, Saudi Arabia; and the Institut National de la Recherche Scientifique, University of Quebec, Montreal, QC, Canada. Since 2015, he has been a Professor with Sun Yat-sen University. He holds two patents granted in China. His research interests are in the general area of 5G wireless communications, and in particular the design and performance analysis of multiantenna systems, cooperative relaying systems, and cognitive relaying networks, and recently focus on the design and analysis of wireless power transfer and/or energy harvesting systems, as well as massive MIMO and small cells.

Dr. Xia received the Professional Award at the IEEE TENCON, held in Macau, in 2015. He was also recognized as an Exemplary Reviewer by the IEEE TRANSACTIONS ON COMMUNICATIONS in 2014, the IEEE COMMUNICATIONS LETTERS in 2014, and the IEEE WIRELESS COMMUNICATIONS LETTERS in 2014 and 2015.

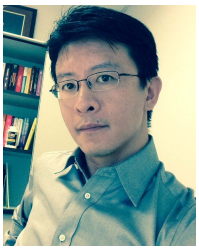

Kaibin Huang (M'08–SM'13) received the B.Eng. (Hons.) and M.Eng. degrees from the National University of Singapore, and the Ph.D. degree from The University of Texas at Austin (UT Austin), all in electrical engineering.

Since 2014, he has been an Assistant Professor with the Department of Electrical and Electronic Engineering (EEE), The University of Hong Kong. He was a Faculty Member with the Department of Applied Mathematics (AMA), The Hong Kong Polytechnic University (PolyU), and the Department of EEE, Yonsei University, South Korea, where he is currently an Adjunct Professor with the School of EEE. His research interests focus on the analysis and design of wireless networks using stochastic geometry and multiantenna techniques.

Dr. Huang held a University Visiting Scholarship with Kansai University, Japan, in 2017. He received the 2015 IEEE ComSoc Asia Pacific Outstanding Paper Award, the Outstanding Teaching Award from Yonsei, Motorola Partnerships in Research Grant, the University Continuing Fellowship from UT Austin, and the Best Paper Award from the IEEE GLOBECOM in 2006 and PolyU AMA in 2013. He frequently serves on the technical program committees of major IEEE conferences in wireless communications. He served as the Lead Chair for the Wireless Communication Symposium of the IEEE Globecom 2017 and the Communication Theory Symposium of the IEEE GLOBECOM 2014, and as the TPC Co-Chair for the IEEE PIMRC 2017 and the IEEE CTW 2013. He was an Editor of the IEEE JOURNAL ON SELECTED AREAS IN COMMUNICATIONS (JSAC) Series on Green Communications and Networking from 2015 to 2016, the IEEE WIRELESS COMMUNICATIONS LETTERS from 2011 to 2016, and the IEEE/KICS JOURNAL OF COMMUNICATION AND NETWORKS from 2009 to 2015. He is currently an Editor of the IEEE TRANSACTIONS ON GREEN COMMUNICATIONS AND NETWORKING and the IEEE TRANSACTIONS ON WIRELESS COMMUNICATIONS. He edited the JSAC 2015 Special Issue on Communications Powered by Energy Harvesting. He was an elected member of the SPCOM Technical Committee of the IEEE Signal Processing Society from 2012 to 2015.

Yik-Chung Wu (S'99–M'05–SM'14) received the B.Eng. and M.Phil. degrees from The University of Hong Kong (HKU) in 1998 and 2001, respectively, and the Ph.D. degree from Texas A&M University, College Station, TX, USA, in 2005, under the Croucher Foundation Scholarship in 2002. From 2005 to 2006, he was a Member of Technical Staff with Thomson Corporate Research, Princeton, NJ, USA. He was a Visiting Scholar with Princeton University, in 2011 and 2015. Since 2006, he has been with HKU, currently as an Associate Professor. His research interests are in general areas of signal processing, machine learning and communication systems, and in particular distributed signal processing and robust optimization theories with applications to communication systems and smart grid. He served as an Editor of the IEEE COMMUNICATIONS LETTERS. He is currently an Editor of the IEEE TRANSACTIONS ON COMMUNICATIONS and the *Journal of Communications and Networks*.